
Article:
Motaman, S, Mullis, AM, Cochrane, RF et al. (2015) Numerical and Experimental Investigations of the Effect of Melt Delivery Nozzle Design on the Open- to Closed-Wake Transition in Closed-Coupled Gas Atomization. Metallurgical and Materials Transactions B. ISSN: 1073-5615

https://doi.org/10.1007/s11663-015-0346-6

Numerical and experimental investigation of the effect of melt delivery nozzle design on the open- to closed-wake transition in closed-coupled gas atomization.

Shahed Motaman, Andrew M. Mullis and Robert F. Cochrane

Institute for Materials Research

University of Leeds, Leeds, UK, LS2 9JT

Duncan J. Borman

School of Civil Engineering

University of Leeds, Leeds, UK, LS2 9JT

Abstract,

The single-phase gas flow behaviour of a Closed Coupled Gas Atomization (CCGA) was investigated with four different melt nozzles tip designs with two types of gas die. Particular attention was paid to the open- to closed-wake transition. Experimental Schlieren imaging and numerical modelling techniques were employed, with good agreement between the two being found in relation to the Wake Closure Pressure (WCP). It was found that the melt nozzle tip design had a significant impact on the WCP, as did the type of die used, with a Convergent-Divergent (C-D) gas die giving significantly high wake closure pressures.

I. Introduction

The gas atomization process, particularly Closed Coupled Gas Atomization (CCGA), is an efficient method for the production of ultra fine, highly spherical metal powders. In principle CCGA is straightforward, high pressure gas jets impinging upon a molten metal stream are used to disrupt the stream, breaking it into a spray of fine droplets. The gas is delivered via a die that will typically be of either the annular slit or discrete jet type. In an annular slit die the gas pass through a narrow channel between the die and the outer surface of the melt delivery nozzle, while in a discrete jet die the gas is delivered through holes machined directly into the die. Liquid metal is then fed down the central bore of the melt delivery nozzle, wherein it wets the nozzle tip (a process termed pre-filming, which is itself dependent upon the gas flow conditions) and is stripped off the circumferential edge of the nozzle by the gas (see figure 1). However, due to hydrodynamic and thermal interaction between the high-pressure gas jets and molten metal stream, especially near the tip of the melt delivery nozzle, the technique is in practise very complex and challenging for both academic understanding and industrial practice. The gas flow pattern around the melt delivery nozzle plays a crucial role in the gas atomization process and may affect the particle size distribution and atomization efficiency.

In previous studies the gas flow pattern around the melt delivery nozzle has been divided into two parts: the near field and the far field regions. The near field is an area about 3 to 4 D (D being the diameter of the tip of the melt delivery nozzle at which pre-filming occurs, (see figure 1) downstream of the melt nozzle tip and in which primary break-up occurs. Beyond this is referred to as far field and is the region in which secondary break-up occurs.

Typical gas flow patterns for a close-coupled atomizer are shown in Figure 1. The gas exiting the die is under-expanded and upon encountering the low pressure region near the melt delivery nozzle will expand rapidly before compressing again, forming a series of

recompression shocks. The reflection of the expansion wave from the sonic boundary will form an internal shock wave at the tip of the melt delivery nozzle. The region of recirculating subsonic gas directly below the melt nozzle and bounded by the sonic boundary and recompression shocks is the wake region, also sometimes referred to as the recirculation zone. It is here that primary breakup occurs.

Various studies, including those by Anderson et al. [1, 2], Ting et al. [3] and Mates et al. [4, 5] have observed two possible forms for the wake region depending upon the gas inlet pressure. At high gas pressure the internal shocks expand downstream in front of the melt delivery nozzle, crossing to form a Mach disk. This gives rise to high pressure at the atomization tip and is termed the closed-wake condition. Conversely, at lower gas inlet pressure a Mach disk will not be present, leading to the open-wake condition, which gives a region of low pressure at the melt delivery nozzle tip. They observed that the wake shape in front of the melt nozzle tip affects the atomization process by increasing the over-ambient pressure in the wake region in the closed-wake condition and hence decreasing the melt flow rate inside the melt delivery nozzle. Conversely, the open-wake condition causes sub-ambient pressure in the wake region and increases the melt flow rate inside the melt delivery nozzle. The gas pressure above which the wake region is in the closed condition, and below which it is in the open condition, is termed the wake closure pressure (WCP).

Mates et al. [4, 5], Anderson et al. [6] and Ting et al. [3, 7] have reported the WCP to be dependent on a variety of parameters such as: gas die inlet pressure, gas die apex angle and the external geometry of the melt delivery nozzle. In addition, they observed that different gas die designs, for instance the use of choked jets or those with a convergent-divergent (C-D) profile, could affect the gas flow field at the melt delivery nozzle tip and consequently the WCP. For gas jets in which the internal profile is cylindrical, or purely convergent, choked flow will occur, with a maximum exit velocity of Mach 1 and rapid, unconstrained expansion

of the gas upon exit. Conversely, for a C-D jet efficient expansion of the gas inside the jet permits a controlled expansion of the gas with supersonic exit velocity. For a given operating pressure the mass flow rate is normally determined by the outlet area for a plain jet and by the throat area (the region of minimum cross section where the profile changes from convergent to divergent) for a C-D jet. The mass flow rates can therefore be significantly different between the two geometries unless the pipe/throat diameters have been selected accordingly.

Wake closure is an area of interest in the study of gas atomization because, as reported by Ting et al. [3], it is believed that operating the system at a pressure just above the WCP is beneficial for producing finer and more uniform powders. A number of researchers have therefore investigated the factors affecting WCP, both experimentally and numerically.

Mi et al. [8] compared the results of numerical simulation of gas–only flow around a melt nozzle with experimental data. The variation of recirculation zone length, wake closure pressure and Mach disk formation with atomization gas pressure were investigated with good agreement being found between the simulations and experimental data. They demonstrated the gas flow behaviour around the melt nozzle is a strong function of atomization gas pressures. Moreover, their numerical results indicated that the open- to closed-wake transition is strongly affected by changing the melt nozzle length. Tong et al. [9] and Xinming et al. [10] reported a comparison of numerical and Schlieren imaging studies on the WCP as a function of atomization gas pressures using an annular slit C-D die. They used a flat tipped melt delivery nozzle and showed the numerical simulation of the gas flow field to be in a good agreement with images obtained with the same nozzle and die design in Schlieren imaging experiments, although they found that the experimentally determined WCP was systematically slightly higher than in the numerical simulations.

Ting et al. [7] have presented a CFD study of the open to closed-wake transition in the CCGA process. They numerically modelled single-phase gas flow around a flat tipped melt nozzle with a choked gas die as a function of gas pressures. Their numerical results showed two separate zones of primary and secondary recirculation zone in front of the melt delivery nozzle, together with Mach disk formation in the closed-wake condition.

Mates et al. [4, 5] have used the Schlieren imaging technique to study single-phase gas flow around a melt delivery nozzle with a flat tipped head and with two die types, one with convergent jets and the other with C-D jets. They observed the open- to closed-wake transition via the formation of a Mach disk at a gas pressure of 5.2 MPa for the convergent gas die, but reported the open-wake condition persisted for the C-D gas die to pressure above 5.2 MPa.

Where the effect of melt nozzle geometry has previously been studied on the open- to closed-wake transition this has been as a function of the external nozzle geometry. This paper presents a study in which the Schlirern imaging technique and CFD simulation for single-phase gas flow are used to investigate the open- to closed- wake transition for four different melt nozzles, all of which have same external geometry, but with different internal profiles. Furthermore, both choked and C-D gas dies were used in combination with these melt nozzles and the results compared.

II. Experimental process

To visualise the gas flow around the melt delivery nozzle an analogue atomizer has been constructed to study the single-phase gas flow as a function of die and nozzle geometry in absence of a second, atomized, fluid (i.e. metal). The Töpler Schlieren lens arrangement has been chosen for observing the gas flow field. Air was used as the atomizing gas and was supplied from four 0.08 m^3 cylinders with maximum pressure of 20 MPa. The cylinders were

connected to the inlet side of a high-pressure regulator to supply a steady gas flow to the gas die at pressures up to 5 MPa. A schematic view of the analogue atomizer and Töpler Schlieren set-up is shown in Figure 2. The Schlieren images were recorded with a high speed digital motion analyzer operating at a frame rate of 15000 fps and a resolution of 750×750 pixels. The field of view during these experiments was typically from the nozzle exit to 10 D downstream from the nozzle exit and the duration of each experiment was about 3.5 seconds. This running time was chosen due to the maximum recording time of the high-speed camera at the selected image resolution. This imaging confirmed that the gas flow was extremely steady throughout the duration of the experiment and for this reason we have used selected stills as being representative of the flow.

The gas die systems for both choked flow and C-D flow comprise a discrete jet arrangement with 18 holes and an apex angle of 45 degrees. The C-D die was designed with a throat diameter of 0.4 mm and an exit diameter of 0.68 mm. Standard isentropic flow theory then gives the gas exit velocity as Mach 2.6 with the ratio of inlet/outlet pressure as 19.95, giving an ideal operating pressure of ~2 MPa (assuming the outlet is at standard atmospheric pressure). The 18 C-D jets were machined into the blank die by first drilling a cylindrical pilot hole to the throat diameter. The die was then placed on a specially constructed gimbal with EDM machining being used to open the outlet of the jet to the desired diameter. This is achieved by rotating the EDM wire at an angle offset from that of the axis of the pilot hole. Four different melt nozzle designs (designated here type 1 to 4) were made from brass and mounted on the analogue atomizer. Figure 3 show the detail of the various geometries considered for the melt delivery nozzles in this study, gives a schematic view of nozzle/die assembly and shows the choked and C-D gas jet profile.

III. Numerical model procedure

The commercial CFD code ANSYS Fluent 13 was used to solve the set of mass, energy and momentum conservation (Reynolds Navier-Stokes) equations using a finite volume approach. Based on the Schlieren imaging study, in which very steady flow was observed, solutions were restricted to the steady-state case. A range of different two-equation turbulence models were applied during the investigation, with the results being relatively insensitive to the choice made, providing confidences in the numerical calculations presented. The SST k-ω model has been applied in the results presented here to close the Reynolds stress terms in the turbulence model. The CFD sensitivity to the turbulence model used is considered in more detail by Motaman et al. [11]. The molten metal was omitted from the model as the aim of this study is to understand the simplified situation of the high-velocity gas jet flow behaviour around the melt delivery nozzle. The SIMPLE algorithm was applied with an implicit 2^{nd} order upwind scheme to solve the governing equations. The governing equations were solved for the r-z components of a cylindrical system which is independent of φ, this having previously have been shown to be a reasonable approximation in this case by Ting et al. [7], Mi et al. [8] and Tong et al. [9]. The computation domain and the nozzle outlined are shown in Figure 4, with the flow direction being from left to right.

In order to evaluate the effect of meshing on the CFD results a series of high-quality meshes were developed on the numerical domain with increasing spatial resolution of 9000, 11000 and 18000 elements. It was established that the results where the mesh containing 11000 elements or more were acceptably mesh independent and these were subsequently used for the simulations reported here. More details of mesh independence study are discussed in Motaman et al. [11].

A range of atomization gas pressures from 1 to 5.5 MPa were considered for the pressure inlet boundary condition to the gas inlet (in the case of the C-D die gas pressures below 2 MPa lead to an over-expanded flow, while pressures above 2 MPa lead to an under-expanded flow). The outlet of the domain (down stream of the melt nozzle) was taken as a pressure condition at atmospheric pressure. The outer boundaries for the chamber, melt delivery nozzle and the gas die were considered as a wall with no-slip velocity condition. For the boundary labelled 'Upper domain boundary' in Figure 4, two boundary models were considered, a wall with no-slip condition and an atmospheric pressure outlet. Calculations have been undertaken for both types of boundary condition. It was found that the results were comparable for both boundary conditions and, as such, the wall boundary was used since this provided more consistent convergence. In addition, for the thermal boundary condition, at the upper boundary flow inlet and outlet, the gas temperature was set at 300 K. In summary, the assumptions made in regard of the numerical model may be stated as follows:

1- Flow is considered to be steady-state.

2- The effects of gravity are neglected.

3- Flow is 2D axis-symmetric.

4- Flow is considered as air and modelled as a compressible ideal gas.

5- The impact of the molten metal is not considered.

IV. Results

A. Schlieren imaging of gas flow with the choked (Cylindrical) die

Analogue atomization experiments were undertaken for each of the four nozzle types, with both the choked (cylindrical) and C-D gas delivery dies, at pressures of 1-5 MPa, with the pressure being increased in 0.5 MPa increments. Figure 5 (upper figure) shows a still set of images of the gas flow around nozzles type 1 to 4 at gas pressure of 1 MPa with the choked

gas die. At this inlet pressure, upon exiting the die the gas is above ambient pressure, resulting in the generation of a series of oblique shocks around the melt nozzle tip. Theses shocks reduce the gas jet velocity. The gas then cyclically re-accelerates and decelerates to form a set of Prandtl-Meyer waves down-stream from the melt nozzle tip. At this pressure, all nozzles are in open-wake condition.

With increasing gas pressure each of the nozzle types progressively undergoes a transition from the open- to closed-wake condition, although the pressure at which this occurs varies considerably with the internal profile. Nozzle type 4 undergoes this transition first, at a pressure of 3 MPa, followed by type 3 at 3.5 MPa with the highest transition pressure (4.5 MPa) being observed for types 1 and 2 (Figure 5 lower part). The Mach disk is clearly evident in each of the images in the lower section of Figure 5, giving confidence in identifying the closed-wake condition in each case.

B. Schlieren imaging of gas flow with the C-D die

The gas flow pattern for the four nozzles being investigated when used with the C-D gas die at gas pressures of 1 and 5 MPa are shown in Figure 6. At a pressure of 1 MPa (upper figure), an over-expanded flow is expected, with Prandtl-Meyer waves being observed about 3D downstream from the melt nozzle tip. Small diamond shocks around the circumferential edge of the melt nozzle tip are also evident. Broadly similar results are obtained for all pressures below 2 MPa.

On increasing the gas pressure to more than 2 MPa, a different flow pattern is observed. Figure 6 (lower part) shows the observed gas flow pattern at an inlet pressure of 5 MPa; although, as above, the flow pattern is relatively insensitive to the actual pressure applied to the gas die in the range 2 to 5 MPa. The emerging jets are now expected to be under-expanded and Prandtl-Meyer waves can be seen. Interestingly, at all pressures up to 5 MPa,

and irrespective of whether the gas flow is in the over- or under-expanded condition, the system remains in the open-wake condition for all nozzles. On the other hand, it is expected that the closed-wake condition should be observed at sufficiently high pressure and we must conclude that the WCP is above 5 MPa for all nozzle types. However, pressures above 5 MPa were not available within the experimental system used.

Consequently, from the results presented above, we conclude that the transition from the open-to closed-wake condition occurs at significantly higher pressure when using a C-D die, relative to the otherwise identical configuration when using a choked (cylindrical jet) gas die.

C. CFD simulation of gas flow with the choked (cylindrical) gas die

Velocity contours for the four different melt nozzles at an atomization gas pressure of 1 MPa, using the choked gas die are given in Figure 7. For all nozzles the high velocity gas jet can be seen to expand rapidly immediately upon exiting the die. At this pressure, the flow is in the open-wake condition, which we determine from the absence of a Mach disk in front of melt nozzle. Due to the rapid expansion of the gas upon exiting the die, oblique shocks are formed around the melt nozzle tip, which slow down the gas flow in order to match the surrounding atmospheric pressure. The gas then undergoes a series of rapid, cyclic accelerations and decelerations producing a series of Prandtl-Meyer waves along the central axis of the simulation. The velocity field for all nozzles at this pressure is very similar.

Increasing the gas pressure to 2.75 MPa, the recirculation zone for type 1 has extended further down-stream of melt nozzle tip but the flow is still in the open-wake condition. A similar situation was also observed for nozzles 2 and 3 at this pressure (Figure 8). In nozzle type 4, the expansion wave extends down to the central axis, forming a Mach disk and consequently a closed-wake condition was observed in this case. Due to the closed-wake condition the recirculation zone for nozzle type 4 was truncated and two recirculation zones

have emerged, one down-stream of the melt nozzle tip and the other down-stream of the Mach disk (Figure 8). By way of a quantitative validation of the numerical results, the position of Mach disk for nozzle type 4 at an inlet pressure of 3 MPa is shown for both the Schlieren image and CFD simulation in Figure 9, wherein a good agreement may be observed.

At an atomization gas pressure of 3.25 MPa the gas flow in nozzle types 1 and 2 was still in the open-wake condition. However, in nozzle type 3, a Mach disk was formed and the gas flow had transformed from the open- to closed-wake condition. For nozzles type 1 and 2 this transition is observed at 4.75 MPa. Figure 10 shows the closed-wake condition for these nozzles at WCP. In all cases the gas flow pattern in the closed-wake condition shows two recirculation zones, one between the melt nozzle tip and the Mach disk and other down-stream of Mach disk.

D. CFD simulation of gas flow with the C-D gas die

A velocity contour plot for the 4 melt nozzles being investigated when combined with the C-D gas die are depicted in Figure 11 for a gas inlet pressure of 1 MPa. At this pressure, the gas flow is over-expanded. The gas flow down-stream of the melt nozzle is in the open-wake condition, with a series of Prandtl-Meyer waves being formed further downstream. Similar results are observed at all pressures up to 5 MPa (images are not presented), irrespective of whether the gas emerging from the jets is in the over- or under-expanded condition. This is consistent with the experimental data, wherein no significant change in the wake condition was observed with increasing gas pressure. However, by increasing the gas pressure above 5 MPa wake closure was observed in all four nozzles, with the estimated values for the WCP being shown in Table I.

Figure 12 shows the closed-wake condition for all nozzles at WCP for each of melt nozzle in Table I. In nozzles type 1 and 2, the closed-wake condition, as evidenced by the formation of a Mach disk, occurred at 5.30 MPa, while in nozzle types 3 and 4 it occurred at pressures of 5.15 MPa and 5.1 MPa, respectively. It seems that, as with the choked die, the closed-wake condition occurs in nozzle types 1 and 2 at a higher gas pressure than for nozzle types 3 and 4, although the difference in WCP between the four nozzles is much reduced compared to the case in which a choked die is used.

V. Discussion

The experimental and CFD studies show that the most significant difference in WCP was observed between nozzle types 1 and 4. The transition between the open- to closed-wake condition appears to be influenced by the combined effects of the internal profile of the melt nozzle and the shape of the resulting recirculation zone that forms. A useful first step is to clarify how the closed-wake occurs for each nozzle at WCP in terms of considering how the flow behaviour changes as inlet pressure increases. To aid with this explanation, nozzle type 1 has been chosen as a reference case to investigate the flow behaviour leading to WCP. The behaviour of the other nozzles can then be understood relative to this case. In the experimental and CFD study this nozzle was observed to have a WCP of 4.5 MPa and 4.75 MPa respectively for the choked die. The key flow behaviour observed as the pressure is increased towards WCP for nozzle type 1 is outlined in Figure 13.

As seen in Figure 13, at a gas pressure of 1 MPa the open-wake condition is evident; the gas leaves the die and is seen to expand rapidly as it moves away from the die exit. It forms a ‘convex lens’ shape as the flow first expands then contracts. This situation causes recompression shocks to form around the circumferential edge of the melt nozzle tip which reduce the gas velocity. The gas re-accelerates then decelerates forming a set of Prandtl-

Meyer waves along the central axis. It can be seen that a recirculation zone forms just downstream of the melt nozzle tip and beneath the expanding gas jet. Increasing the gas pressure to 2 MPa causes an expansion of the convex lens shape gas wave in both directions (length and width). The recirculation zone, which is surrounded by the expanding gas wave, is squeezed downwards by the expanding gas wave. This causes a change in both shape and size of the recirculation zone compared to the previous lower inlet gas pressure (Figure 13). Finally at the WCP (4.75 MPa) the recirculation zone is pinched-off by the further expansion of the gas wave and a Mach disk is seen to form. The transition to the closed-wake condition is due to the expanding gas increasing in size to the extent that it reconnects with itself on the central axis. It is important to note that this mechanism for the transition from the open- to closed-wake condition is observed to occur in a similar manner (expanding gas wave reconnecting with itself on the central axis) for all nozzle types tested in the experiments, but at different gas pressures.

The open- to closed-wake transition for nozzle type 1 with the C-D gas die also was seen to follow the same trend, but with the C-D gas die always transitioning at a higher WCP. Moreover, the difference between the WCP for the various nozzles considered was much smaller when the C-D die was utilised, relative to that for the choked die. To investigate this behaviour the difference in the gas flow between the choked and C-D gas die (for a given nozzle design) is considered. Figure 14 shows the velocity field for a type 1 nozzle with both a C-D and a choked gas die at the same gas inlet pressures. As noted, a higher WCP is found in the case of the C-D design. The reason for this can be understood in the context of how the wake closure occurs. In the case of the C-D design, upon exiting the die the jet does not expand to the same extent as the choked design, with a more collimated jet for the C-D gas die compared to choked die (Figure 14). This is to be expected, for the choked die the inlet and outlet gas pressures will be the same, whereas for the C-D die the outlet pressure is

approximately 1/20 of the inlet pressure due to the controlled expansion of the gas inside the jet. For both dies, when considered individually, the width of the expanding gas wave increases in an approximately linear manner with jet exit pressure. However, no correlation of expansion wave width with pressure is possible between dies as the exit pressure is very much lower in the C-D die than in the choked die.

In the case of the choked design, the larger width of the expanding wave pinches-off the recirculation zone at a lower gas pressure compared to the C-D gas die (Figure 14), hence the lower WCP. It should be noted that a similar trend is observed for all melt nozzles, regardless of melt tip geometry, with WCP occurring at a higher pressure for the C-D case. This condition is also supported by the argument of Ting et al. [3] that WCP for a C-D gas die was measured at a gas pressure about 5 MPa.

The next step is to consider why WCP depends upon melt nozzle tip design. To do this nozzle type 4 is compared to type 1, as these two show the most significant difference in WCP. Figure 15 compares the velocity vector field for the choked and C-D dies in these two nozzles. The length of the convex-lens shape expanding gas waves for both nozzles designs are not significantly impacted by the change in pressure, being 4.5 mm at 1 MPa and 9 mm at 2 MPa, irrespective of nozzle design. However, the shape of the expansion wave is different. As the gas pressure is increased from 1 to 2 MPa, each nozzle displays a convex-lens shape gas wave that expands in both length and width, but in the type 1 nozzle this is restrict in width.

As also shown in Figure 15, the length and shape of the recirculation zone formed in front of the melt tip is different for the two nozzles. The hemispherical shape of type 4 results in a recirculation zone that produces a flow of gas inside the melt tip cavity. As a result, this changes the direction at which the gas in the recirculation zone meets the incoming gas from

the die (Figure 16). Whether these are causally related or manifestations of the same underlying cause is difficult to establish. The direction in which the recirculating gas meets the incoming gas will alter the momentum balance in this system. Equally, the shape of the melt delivery nozzle influences the formation and direction of oblique shocks at the nozzle tip, which could affect both the recirculation pattern and the down-stream gas expansion wave. In this respect we note that the introduction of convex/concave surface is common practice in the aerospace industry to alter the direction and significance of oblique shocks.

VI. Conclusions

Use of a combination of CFD and Schlieren imaging techniques for observing and simulating the gas flow patterns around the melt delivery nozzle of a Close-Coupled Gas Atomizer has revealed reasonable agreement between the numerical and experimental results in determining the WCP. Observation of gas flow patterns around 4 different melt nozzles and with two gas die systems (choked and C-D) revealed a strong, and perhaps unexpected, effect on WCP which is very sensitive to the even a small change in the melt tip geometry. According to the CFD and the experimental results, the closed-wake condition is achieved with a choked die at atomization gas pressures of 4.5 MPa for nozzle types 1 and 2, 3.5 MPa for type 3 and 3 MPa for type 4. On the other hand, the C-D gas die tested in this investigation, which was designed to produce ideal expansion at an inlet gas pressure of 2 MPa, did not display wake closure with any nozzle until the gas pressure exceeded 5 MPa, and only a very weak dependence of WCP upon nozzle geometry was observed. However, it should be stressed that these result apply to the specific C-D gas die design in this test and the WCP may be different if, for instance, the apex angle or internal profile of the C-D gas die were changed. Although, Ting et al. [3] reported atomizer operation at such high gas

pressures and close to the WCP condition may produces finer particles, it will also increases production costs and gas consumption. Finding the appropriate match of die and nozzle design, and optimising the operating conditions for the pairing, remains a significant challenge for atomizer designers.

This research also proposed a new explanation regarding to open and closed-wake condition for different melt tip design. Building upon the previous model by Ting et al. [3], which laid much of the fundamental understanding of the wake closure phenomenon, the model proposed in this research explains the open- to closed-wake transition as a function of gas die and melt tip design in more details. It was found that the closed-wake condition occurs when the convex-lens shape expanding gas wave expands gradually by increasing inlet gas pressure until it pinches-off the recirculation zone. Comparison between the velocity fields produced by the choked and C-D gas die at the same inlet gas pressure in showed that the convex-lens shape gas wave in the C-D die is more collimated compared to that for the choked gas die, leading to a higher WCP for the C-D die. Comparing the velocity fields between different nozzle types showed the melt tip profile design affects the shape and length of the recirculation zone. As a result, nozzles with an internal cavity (Types 3 or 4 as studied here) help the convex-shaped expanding wave expand further downward to the recirculation zone and pinches-off this region at a lower gas pressure (lower WCP).

References

1. I.E. Anderson, R.S. Figliola and H. Morton, 1991, Materials science and engineering, vol. 148, pp.104-114.

2. I.E. Anderson, R.L. Terpstra, R.S. Figliola, 2004, Advances in powder metallurgy and particulate materials, vol. 2, pp.26-36.

3. J. Ting, M.W. Peretti, W.B. Eisen, 2002, Material Science and engineering, vol. 326, pp.110-121.

4. S.P. Mates, G. S. Settles, 1995, Advances in Powder Metallurgy and Particulate Materials, Metal Powder Industries Federation, vol. 2, pp. 1-15.

5. S.P. Mates, G.S. Settles, 2005, Atomization and spray, vol. 15, pp. 20-27.

6. I.E. Anderson, R.S. Figliola, 1998, Modern Developments Powder Metallurgy, vol. 20, pp. 205-223.

7. J. Ting, I.E. Anderson, 2004, Material science and engineering A, vol. 379, pp. 264-276.

8. J. Mi, R.S. Figliola, I.E. Anderson, 1997, Metallurgical and Materials transactions B. Vol. 28B, pp. 935-941.

9. M. Tong, D.J. Browne, 2009, Computers & Fluids, Vol. 38, pp. 1183-1190.

10. Z. Xinming, J. XU, Z. Xuexin and Z. Shaoming, 2009, Science in China Series E, vol. 52, pp. 3046-3053,

11. S. Motaman, A.M. Mullis, R.F. Cochrane, I. M. McCarthy, D.J. Borman, 2013, Computers & Fluids, vol. 88, pp. 1-10.

Figures Captions

Fig. 1- Schematic diagram of gas-only flow in a CCGA system in the (left) open- and (right) closed-wake conditions.

Fig. 2- Schematic view of the Töpler Schlieren apparatus used to image gas flow in the analogue atomizer.

Fig. 3- Schematic view of (a) the four melt nozzle used in this study, (b) the annular slit die and nozzle configuration in the analogue atomizer (shown for nozzle type 1) and (c) the choked and C-D gas jet profile and the discrete jet arrangement in the gas die.

Fig. 4- The boundary conditions and mesh applied on the numerical domain.

Fig. 5- Schlieren images of the gas flow around the four melt delivery nozzles investigated in this study when used with a choked (cylindrical) die. Upper row shows flow in the open-wake condition at a pressure of 1 MPa, lower row shows flow in the closed-wake condition at the WCP.

Fig. 6- Schlieren images of the gas flow around the four melt delivery nozzles investigated in this study when used with a C-D die. Upper row shows flow at a pressure of 1 MPa, lower row shows flow at a pressure of 5 MPa. All cases are in the open-wake condition.

Fig. 7- CFD Velocity contours (m s^{-1}) for the four melt delivery nozzles investigated in this study when used with a choked (cylindrical) die at a gas inlet pressure of 1 MPa.

Fig. 8- CFD Velocity contours (m s^{-1}) for the four melt delivery nozzles investigated in this study when used with a choked (cylindrical) die at a gas inlet pressure of 2.75 MPa.

Fig. 9-Comparison of the CFD and experimentally determined position of the Mach disk for nozzle type 4 with a choked gas die at an inlet pressure of 3 MPa.

Fig. 10- CFD Velocity contours (m s^{-1}) for the four melt delivery nozzles investigated in this study when used with a choked (cylindrical) die at WCP.

Fig. 11-CFD Velocity contours (m s^{-1}) for the four melt delivery nozzles investigated in this study when used with a C-D die at a gas inlet pressure of 1 MPa (over-expanded flow).

Fig. 12- CFD Velocity contours (m s^{-1}) for the four melt delivery nozzles investigated in this study when used with a C-D die at WCP.

Fig. 13- The velocity vector field, as a function of gas inlet pressure, around a type 1 nozzle when using a choked die.

Fig. 14- Comparison of the velocity vector field, as a function of gas inlet pressure, around a type 1 nozzle, when used with a choked and C-D die.

Fig. 15- Comparison of the velocity vector field, as a function of gas inlet pressure, around a type 1 and a type 4 nozzle, when used with a choked die.

Fig. 16- The schematic view of gas flow and gas jets meeting point for nozzles type 1 and 4 at open- wake condition and atomization gas pressure of 1 MPa.

Table I. The WCP for different melt nozzles with two gases die system.

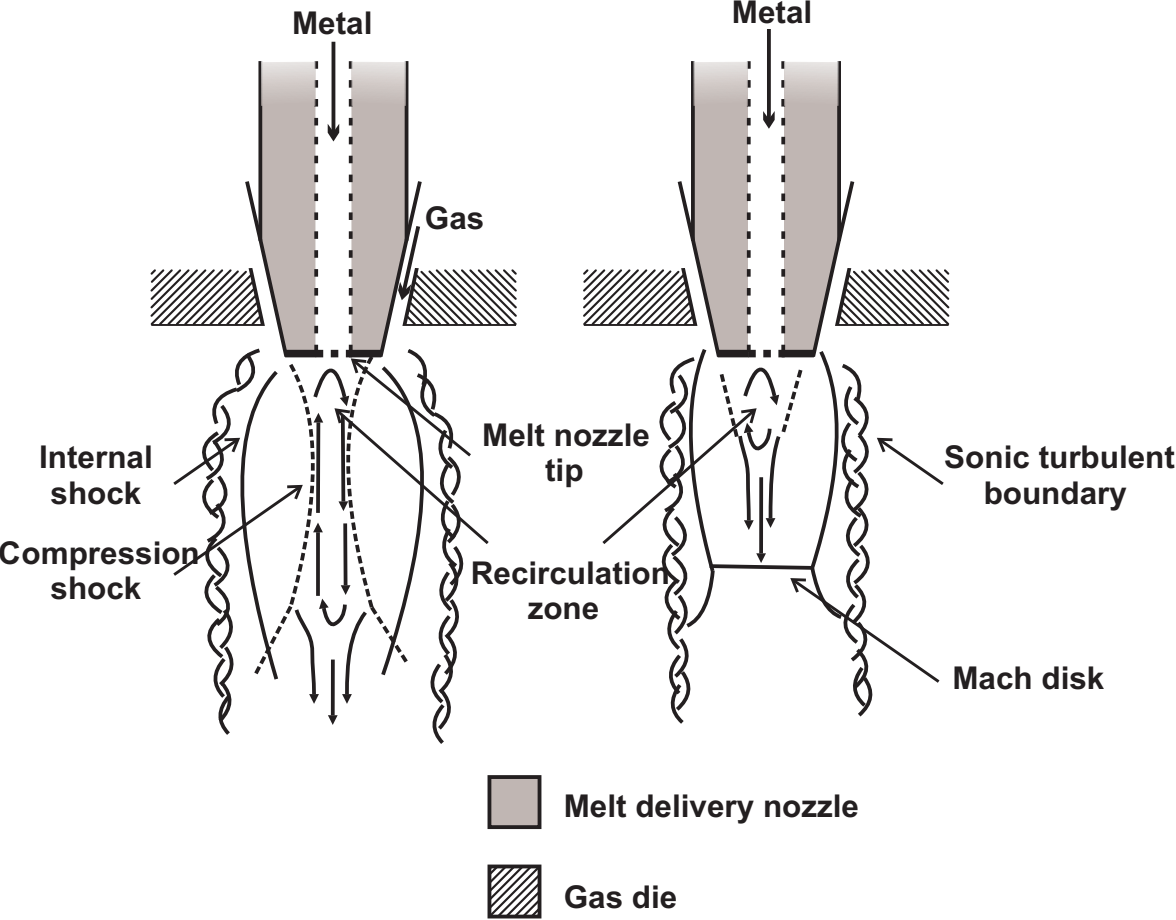
Metal
Gas
Internal shock
Compression shock
Melt nozzle tip
Recirculation zone
Metal
Sonic turbulent boundary
Mach disk
Melt delivery nozzle
Gas die

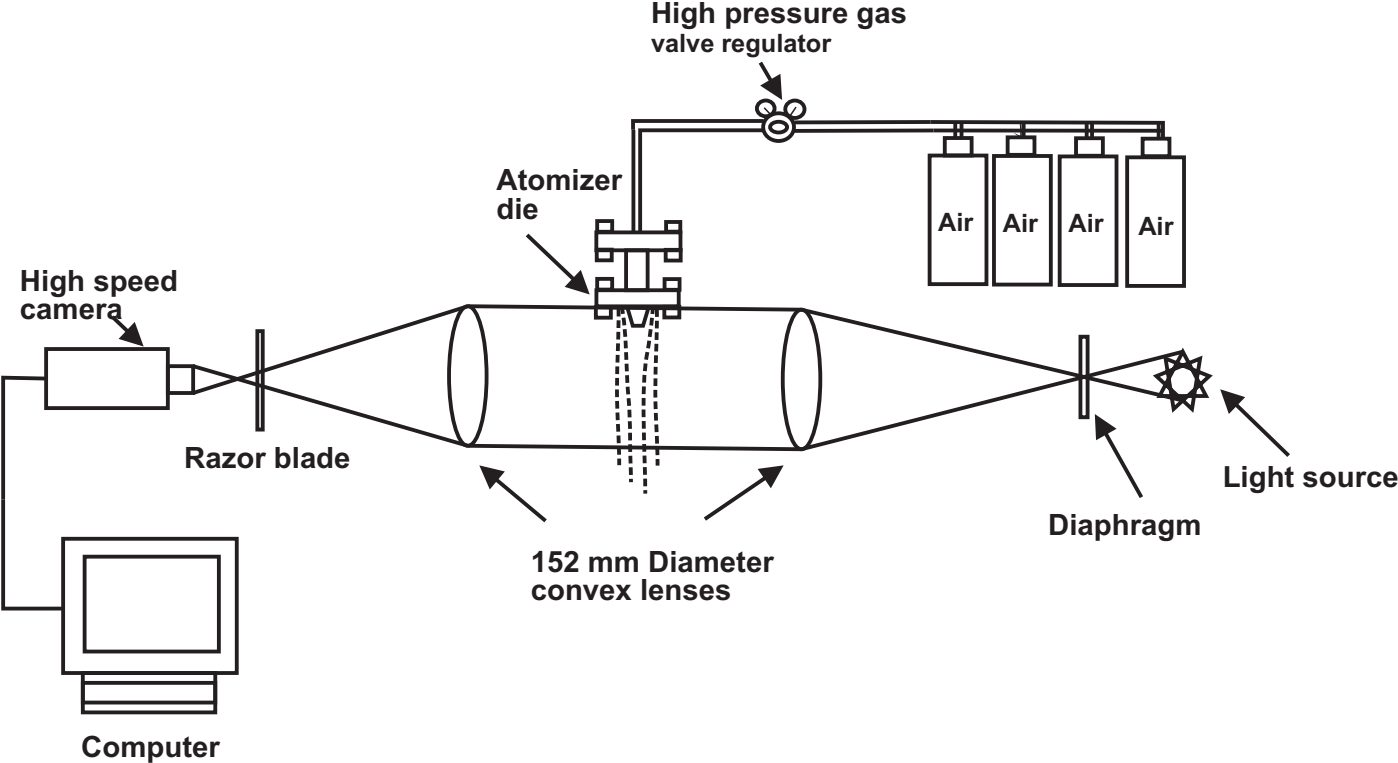
High pressure gas
valve regulator
Atomizer
die
Air
Air
Air
Air
High speed
camera
Razor blade
152 mm Diameter
convex lenses
Diaphragm
Light source
Computer

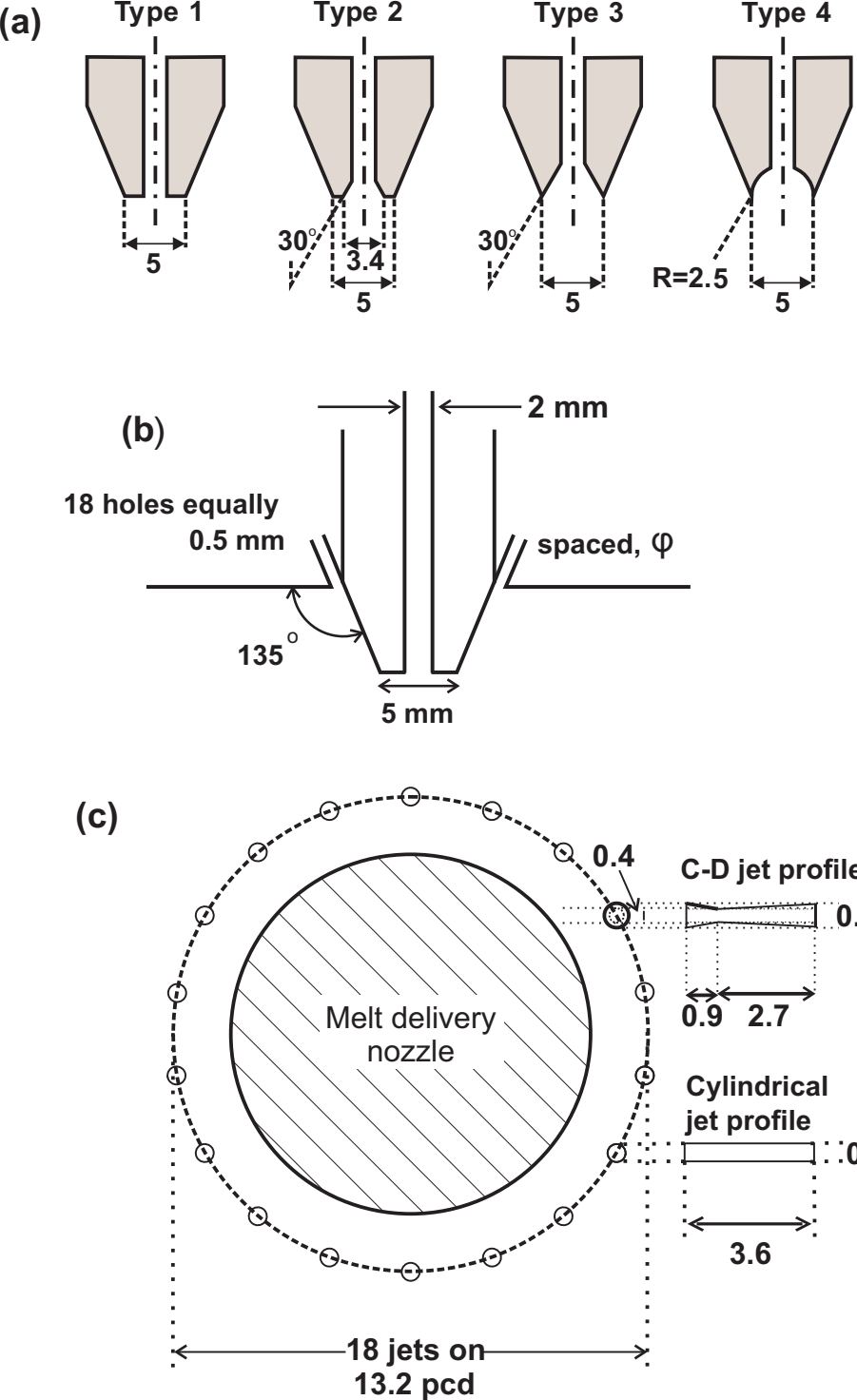
(a)
Type 1
Type 2
Type 3
Type 4
5
30°
3.4
5
30°
5
R=2.5
5
(b)
2 mm
18 holes equally
0.5 mm
spaced, φ
135°
5 mm
(c)
0.4
C-D jet profile
0.680
0.9
2.7
Melt delivery
nozzle
Cylindrical
jet profile
0.4
3.6
18 jets on
13.2 pcd

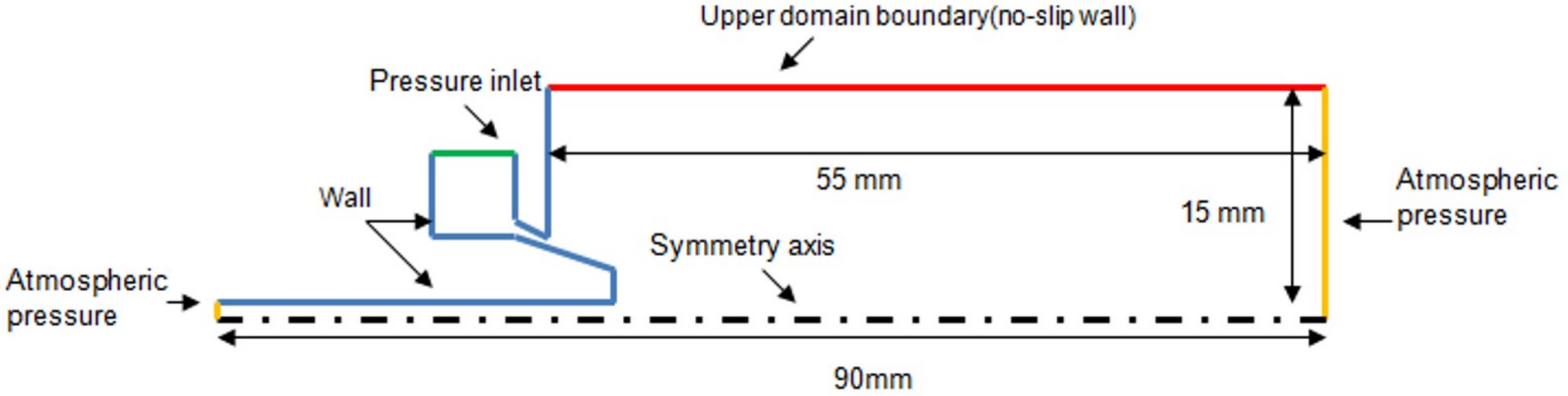
Upper domain boundary(no-slip wall)
Pressure inlet
55 mm
15 mm
Atmospheric pressure
Wall
Symmetry axis
Atmospheric pressure
90mm

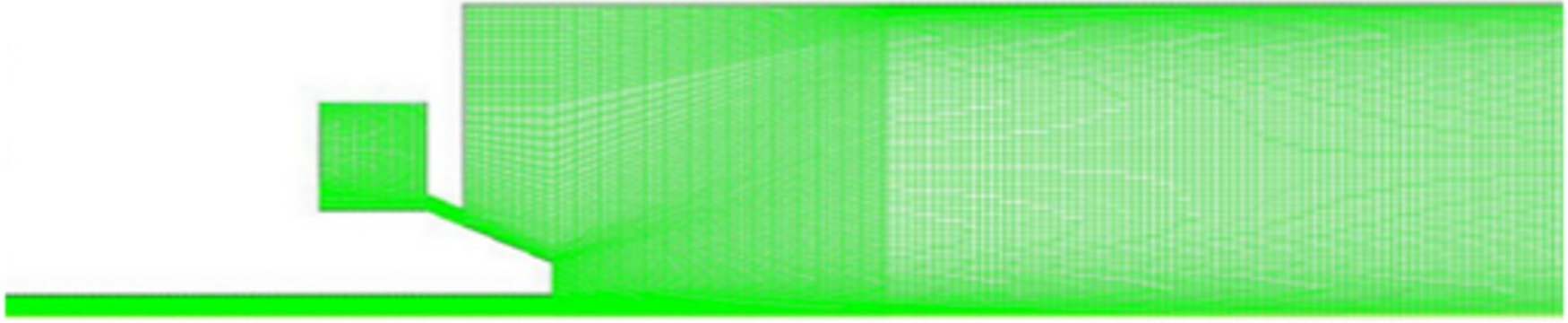

Type 1

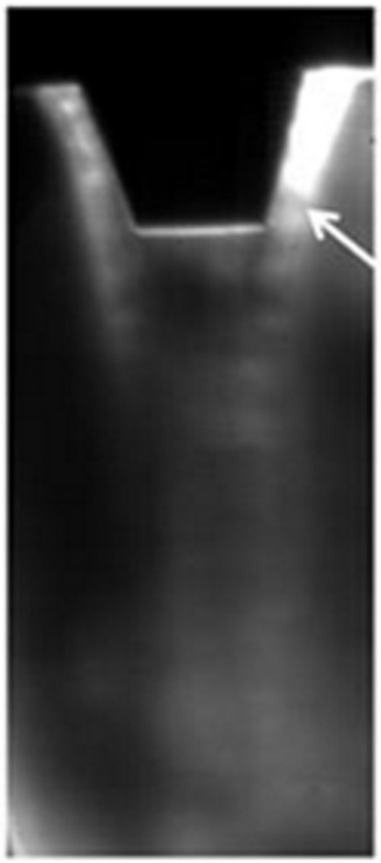

a: 1 MPa

Type 2

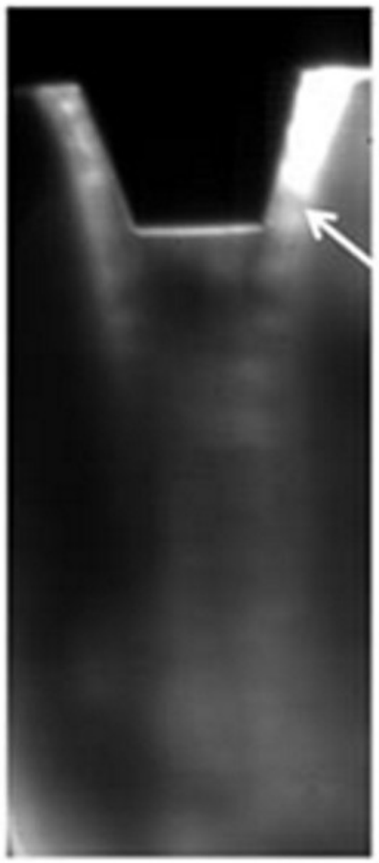

b: 1 MPa

Type 3

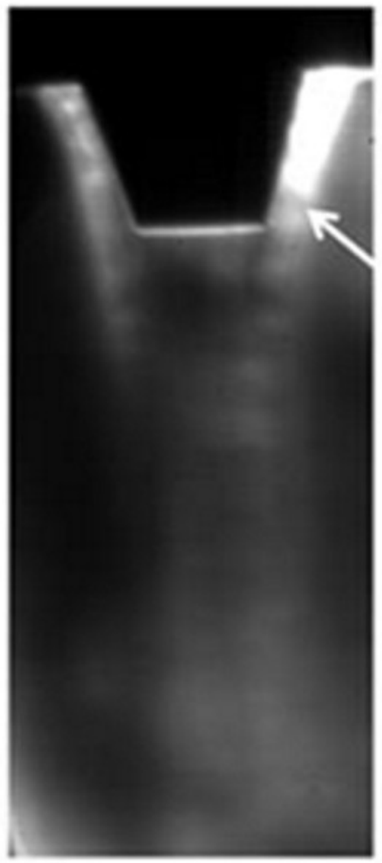

c: 1 MPa

Type 4

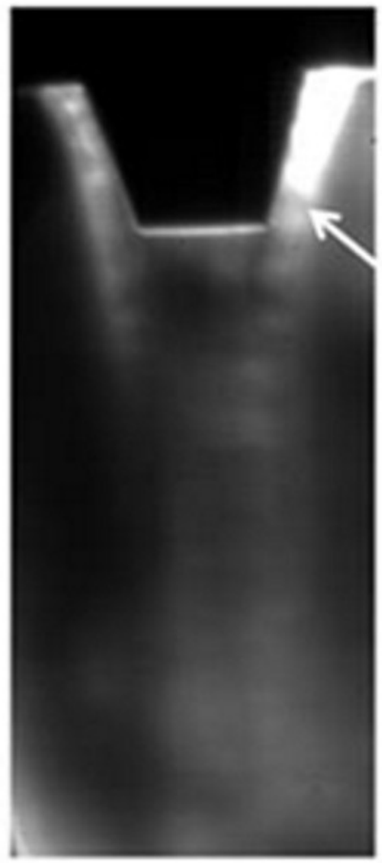

d: 1 MPa

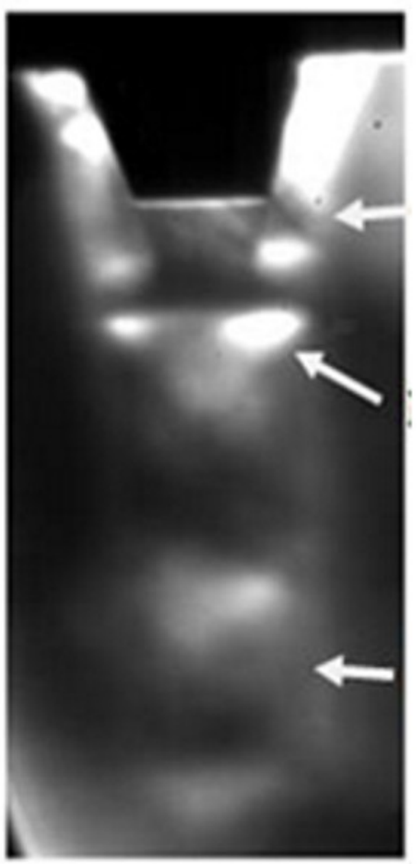

e: 4.5 MPa

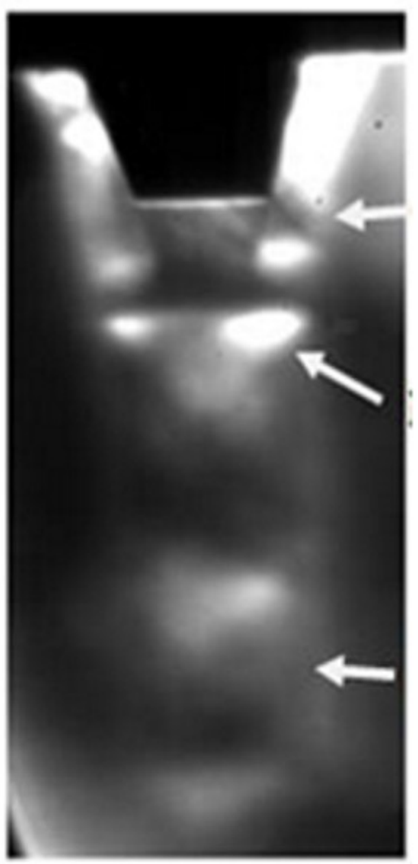

f: 4.5 MPa

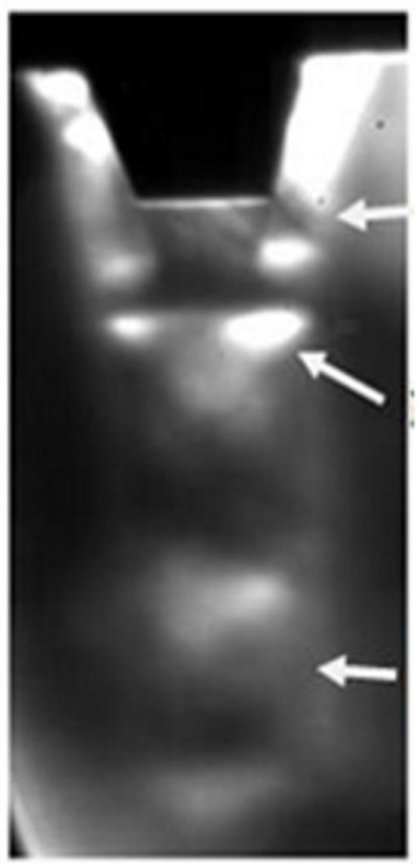

g: 3.5 MPa

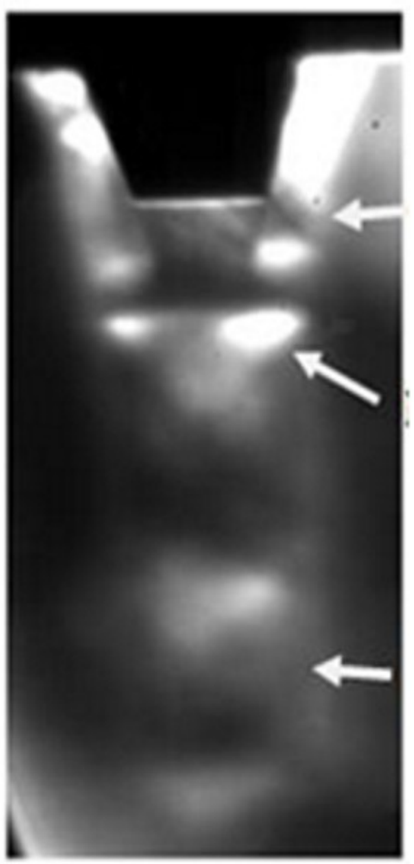

h: 3 MPa

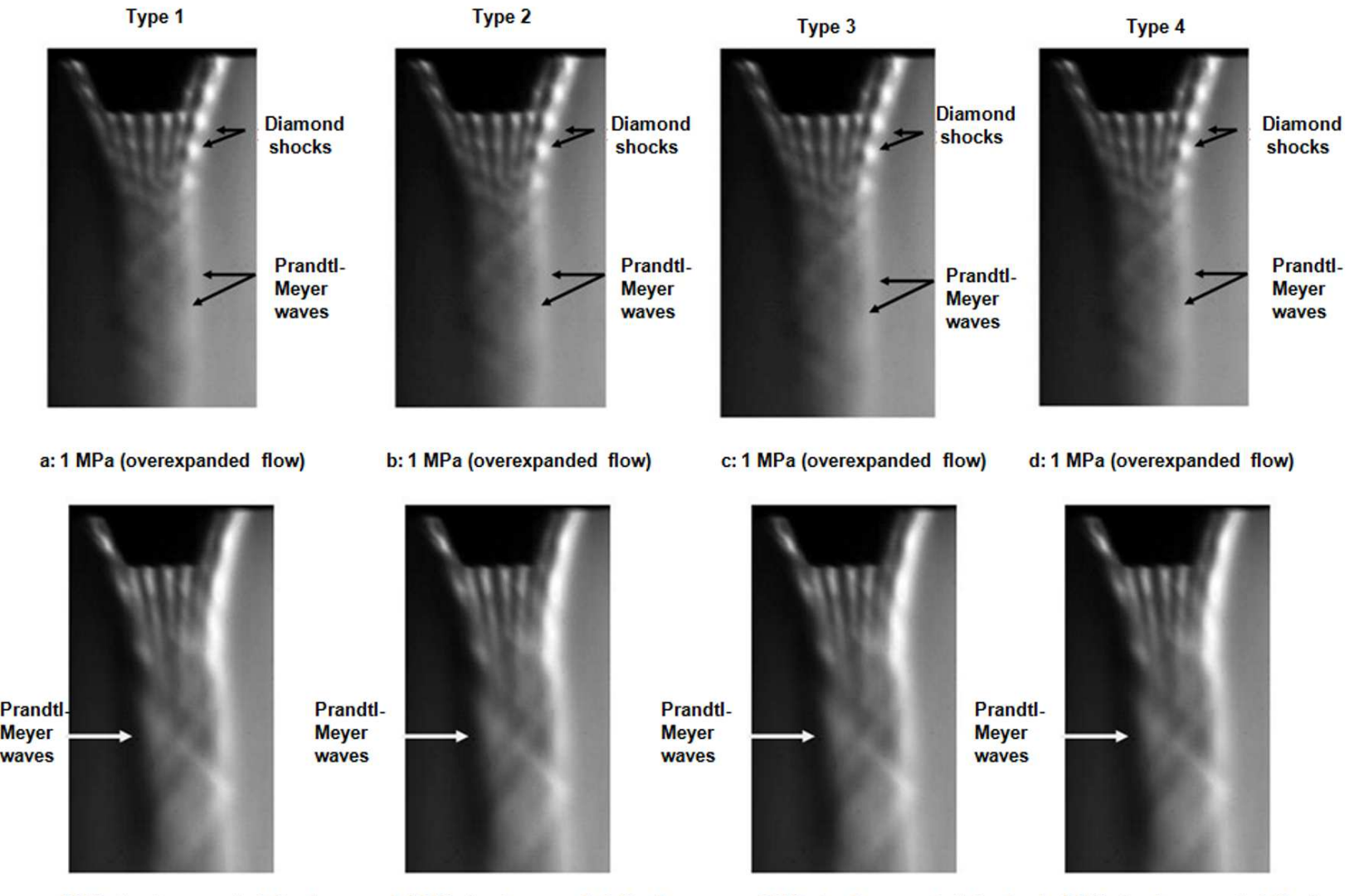

a: 1 MPa (overexpanded flow) b: 1 MPa (overexpanded flow) c: 1 MPa (overexpanded flow) d: 1 MPa (overexpanded flow)

e: 5 MPa (underexpanded flow) f: 5 MPa (underexpanded flow) g: 5 MPa (underexpanded flow) h: 5 MPa (underexpanded flow)

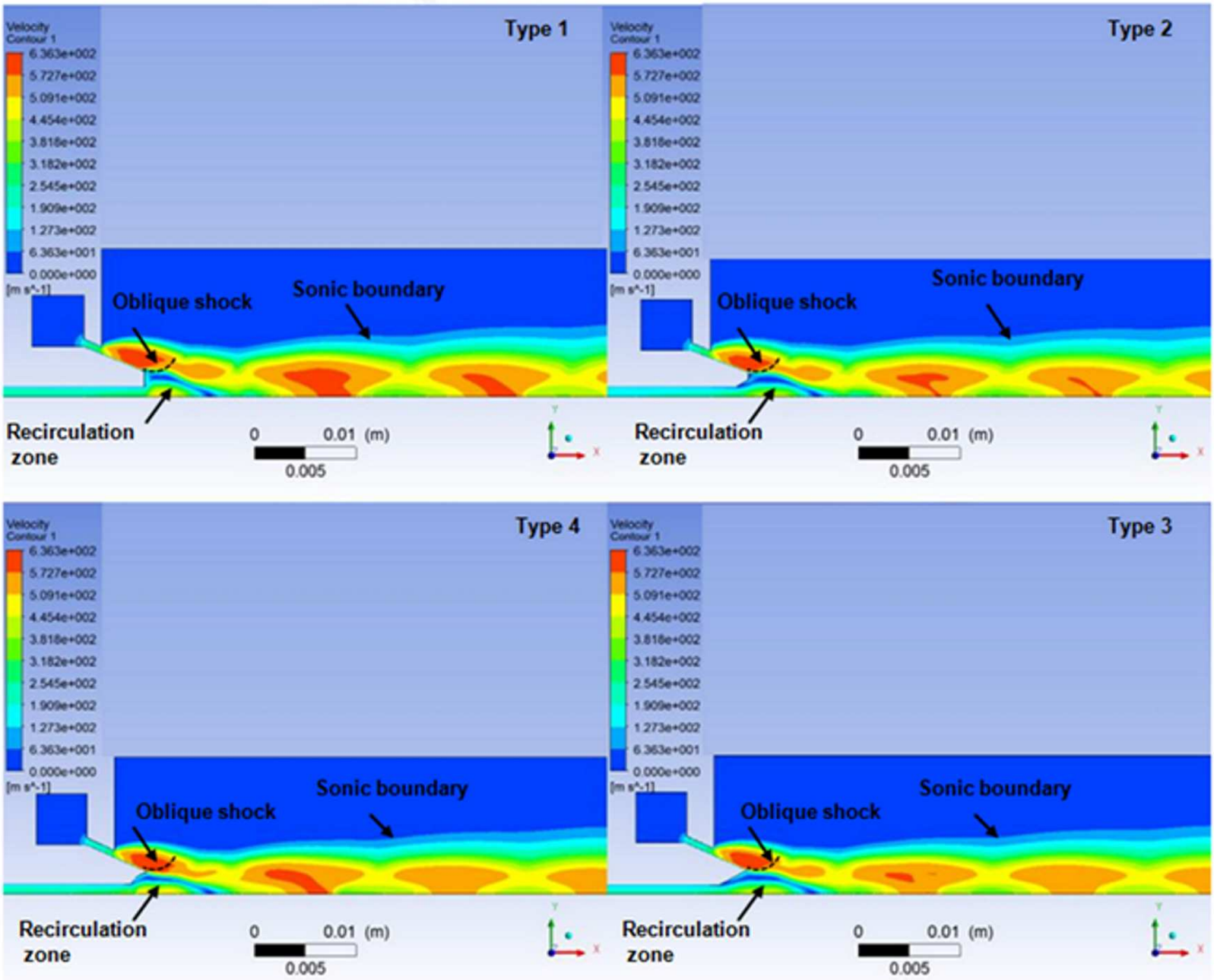
Type 1
Velocity
Contour 1
6.363e+002
5.727e+002
5.091e+002
4.454e+002
3.818e+002
3.182e+002
2.545e+002
1.909e+002
1.273e+002
6.363e+001
0.000e+000
[m s^-1]
Oblique shock
Sonic boundary
Recirculation zone
0
0.01 (m)
0.005
Type 2
Velocity
Contour 1
6.363e+002
5.727e+002
5.091e+002
4.454e+002
3.818e+002
3.182e+002
2.545e+002
1.909e+002
1.273e+002
6.363e+001
0.000e+000
[m s^-1]
Oblique shock
Sonic boundary
Recirculation zone
0
0.01 (m)
0.005
Type 4
Velocity
Contour 1
6.363e+002
5.727e+002
5.091e+002
4.454e+002
3.818e+002
3.182e+002
2.545e+002
1.909e+002
1.273e+002
6.363e+001
0.000e+000
[m s^-1]
Oblique shock
Sonic boundary
Recirculation zone
0
0.01 (m)
0.005
Type 3
Velocity
Contour 1
6.363e+002
5.727e+002
5.091e+002
4.454e+002
3.818e+002
3.182e+002
2.545e+002
1.909e+002
1.273e+002
6.363e+001
0.000e+000
[m s^-1]
Oblique shock
Sonic boundary
Recirculation zone
0
0.01 (m)
0.005

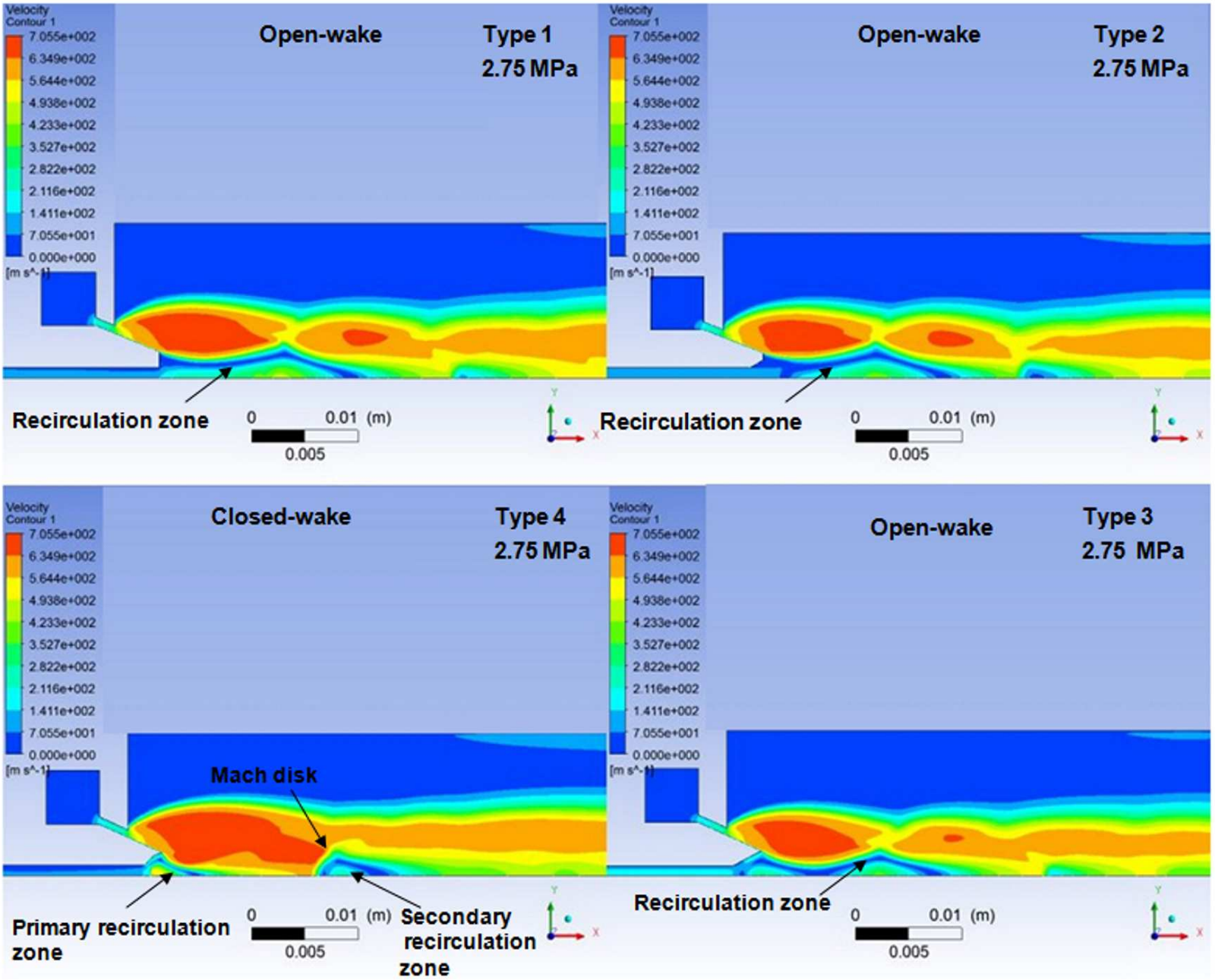
Velocity
Contour 1
7.055e+002
6.349e+002
5.644e+002
4.938e+002
4.233e+002
3.527e+002
2.822e+002
2.116e+002
1.411e+002
7.055e+001
0.000e+000
[m s^-1]
Open-wake
Type 1
2.75 MPa
Recirculation zone
0
0.01 (m)
0.005
Open-wake
Type 2
2.75 MPa
Recirculation zone
0
0.01 (m)
0.005
Closed-wake
Type 4
2.75 MPa
Mach disk
Primary recirculation zone
Secondary recirculation zone
0
0.01 (m)
0.005
Open-wake
Type 3
2.75 MPa
Recirculation zone
0
0.01 (m)
0.005

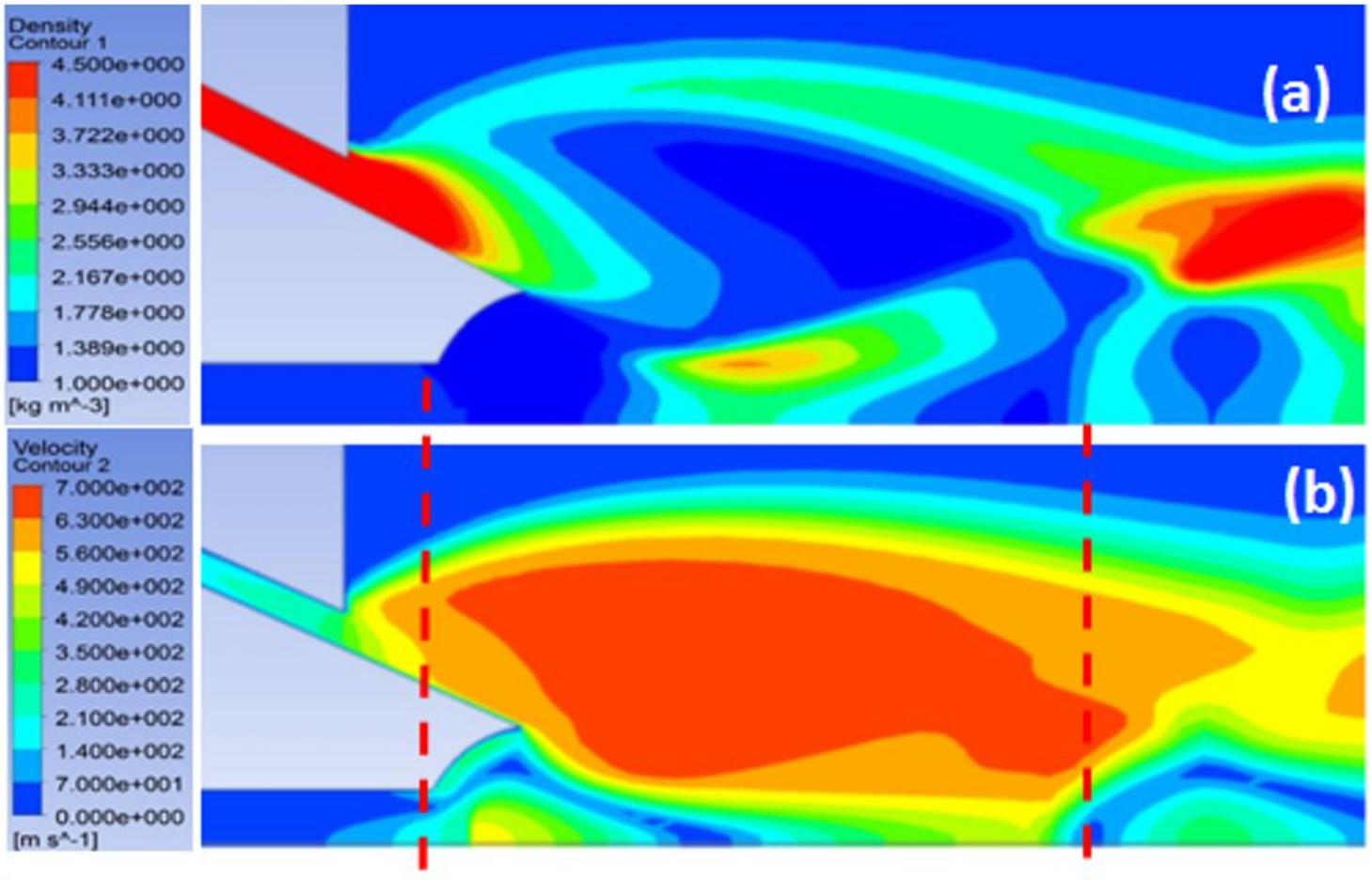
Density
Contour 1
4.500e+000
4.111e+000
3.722e+000
3.333e+000
2.944e+000
2.556e+000
2.167e+000
1.778e+000
1.389e+000
1.000e+000
[kg m^-3]
(a)
Velocity
Contour 2
7.000e+002
6.300e+002
5.600e+002
4.900e+002
4.200e+002
3.500e+002
2.800e+002
2.100e+002
1.400e+002
7.000e+001
0.000e+000
[m s^-1]
(b)

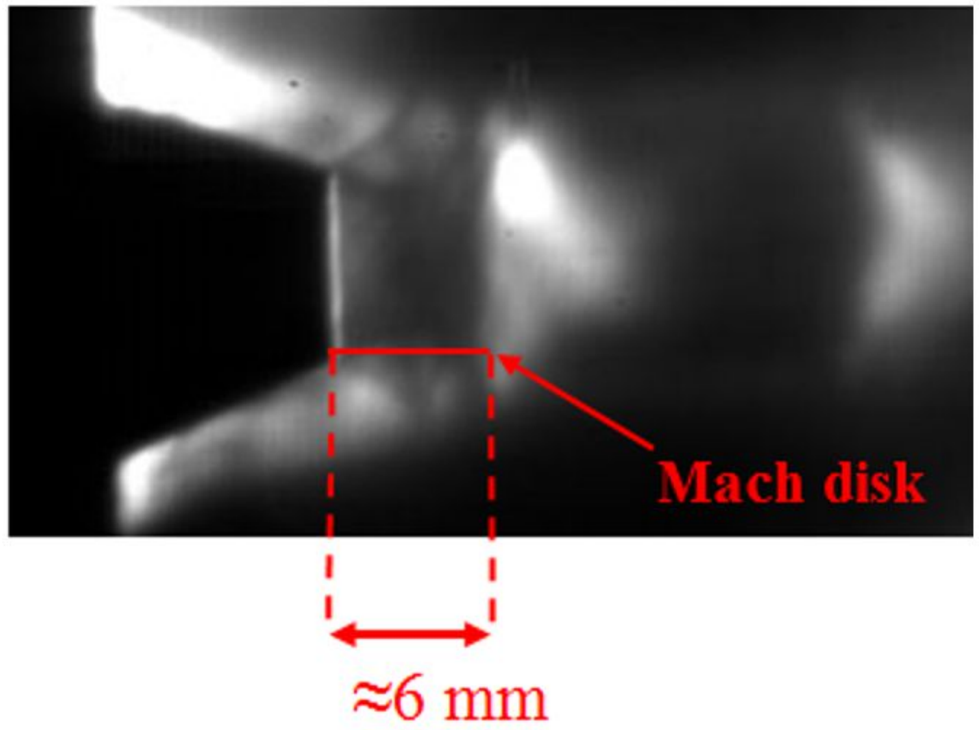
Mach disk
≈6 mm

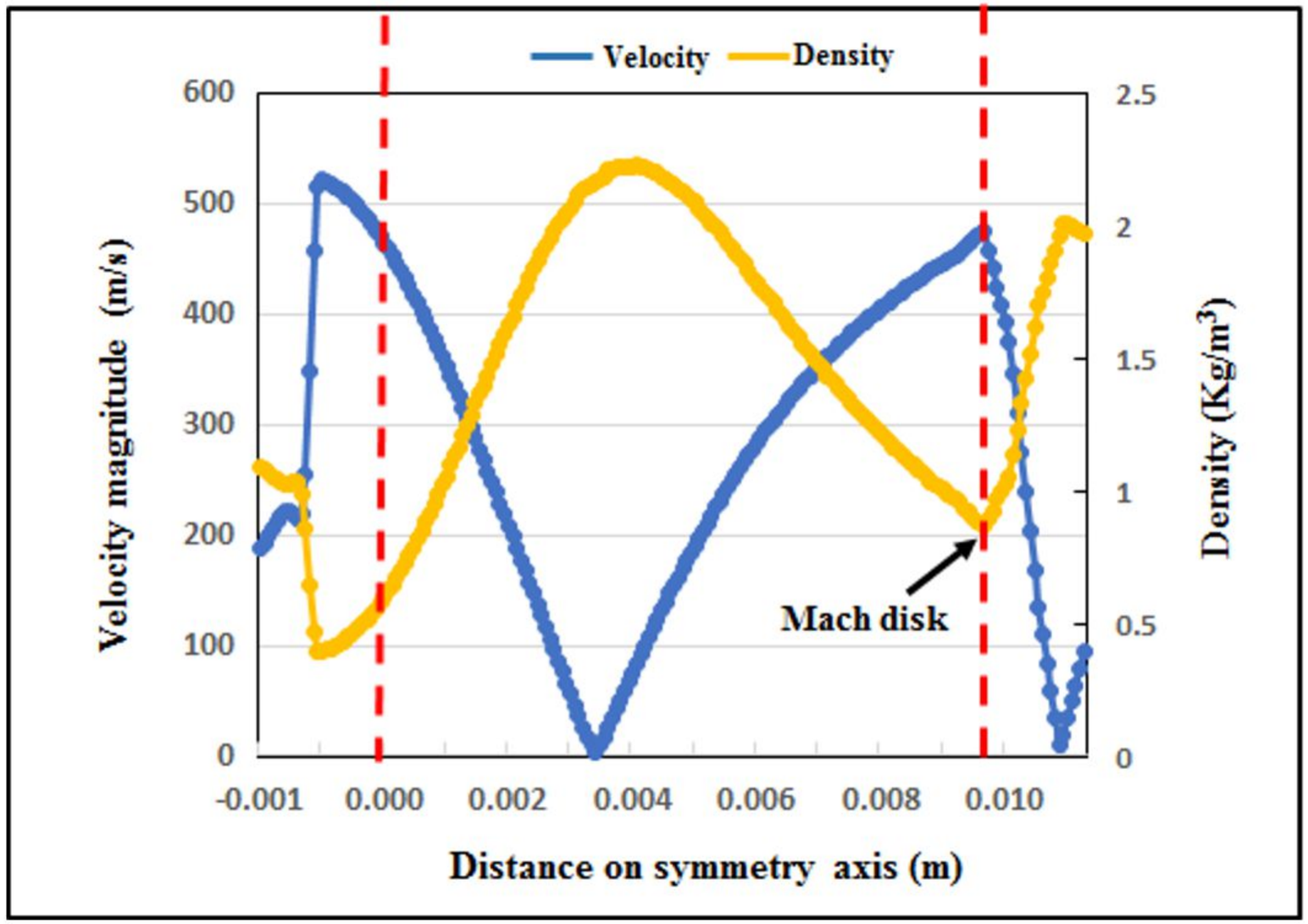
Velocity
Density
600
500
400
300
200
100
0
2.5
2
1.5
1
0.5
0
-0.001
0.000
0.002
0.004
0.006
0.008
0.010
Velocity magnitude (m/s)
Density (Kg/m3)
Mach disk
Distance on symmetry axis (m)

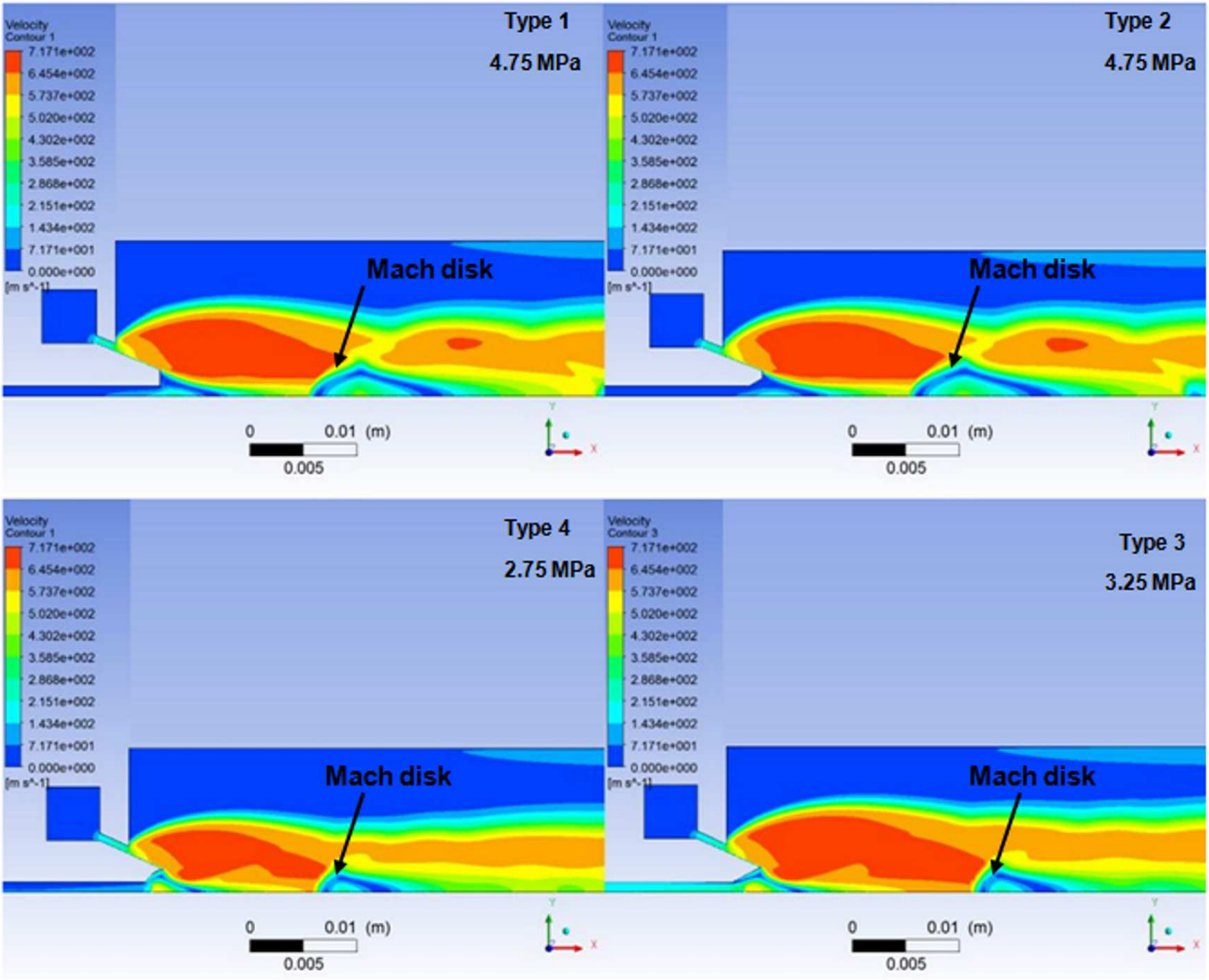
Velocity
Contour 1
7.171e+002
6.454e+002
5.737e+002
5.020e+002
4.302e+002
3.585e+002
2.868e+002
2.151e+002
1.434e+002
7.171e+001
0.000e+000
[m s^-1]
Type 1
4.75 MPa
Mach disk
0
0.01 (m)
0.005
Type 2
4.75 MPa
Mach disk
0
0.01 (m)
0.005
Velocity
Contour 1
7.171e+002
6.454e+002
5.737e+002
5.020e+002
4.302e+002
3.585e+002
2.868e+002
2.151e+002
1.434e+002
7.171e+001
0.000e+000
[m s^-1]
Type 4
2.75 MPa
Mach disk
0
0.01 (m)
0.005
Velocity
Contour 3
7.171e+002
6.454e+002
5.737e+002
5.020e+002
4.302e+002
3.585e+002
2.868e+002
2.151e+002
1.434e+002
7.171e+001
0.000e+000
[m s^-1]
Type 3
3.25 MPa
Mach disk
0
0.01 (m)
0.005

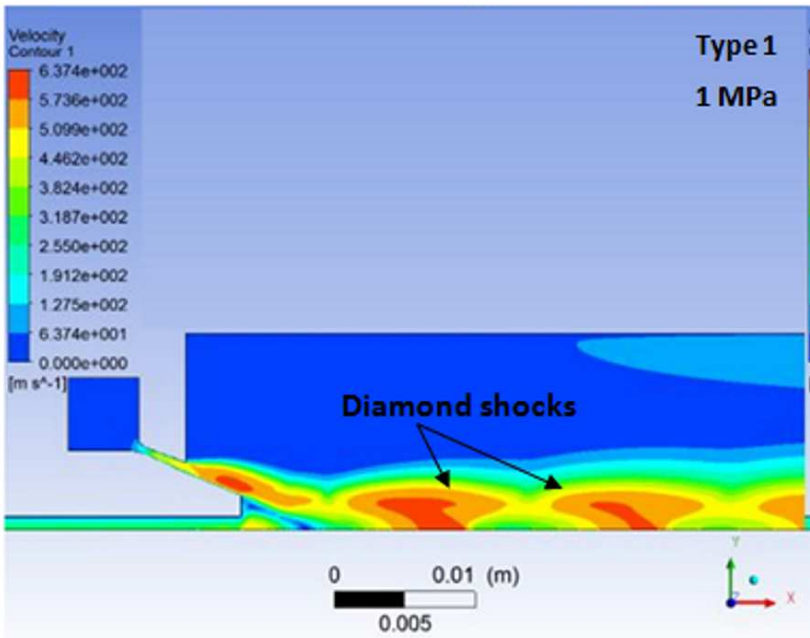
Velocity
Contour 1
6.374e+002
5.736e+002
5.099e+002
4.462e+002
3.824e+002
3.187e+002
2.550e+002
1.912e+002
1.275e+002
6.374e+001
0.000e+000
[m s^-1]
Type 1
1 MPa
Diamond shocks
0
0.01 (m)
0.005
Y
X

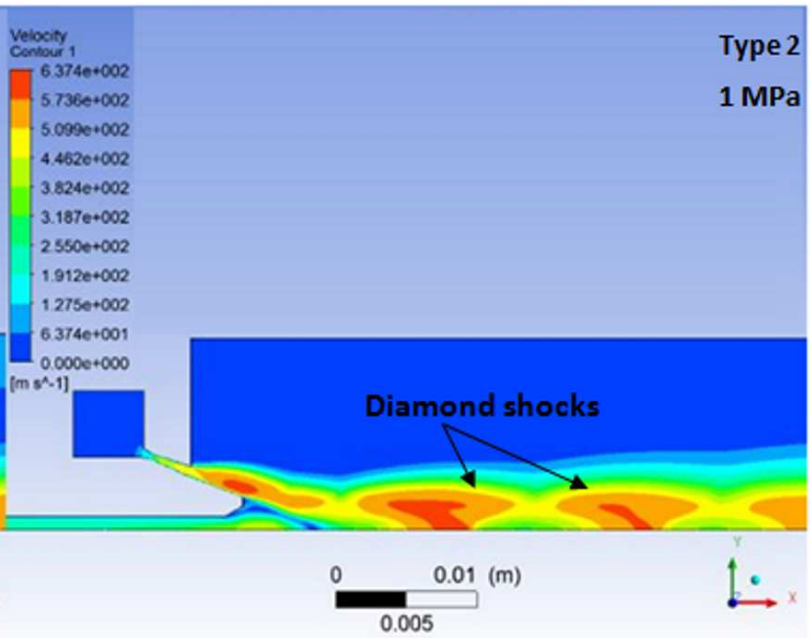
Velocity
Contour 1
6.374e+002
5.736e+002
5.099e+002
4.462e+002
3.824e+002
3.187e+002
2.550e+002
1.912e+002
1.275e+002
6.374e+001
0.000e+000
[m s^-1]
Type 2
1 MPa
Diamond shocks
0
0.01 (m)
0.005
Y
X

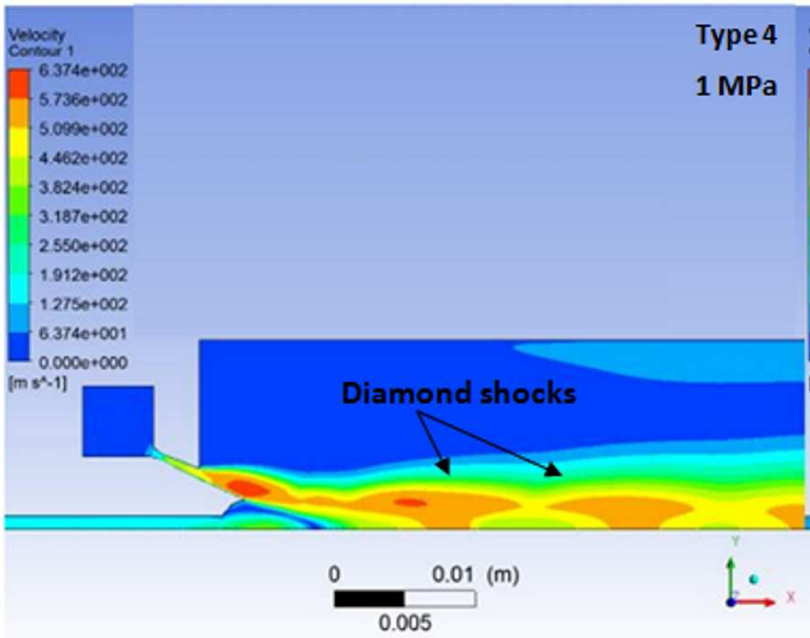
Velocity
Contour 1
6.374e+002
5.736e+002
5.099e+002
4.462e+002
3.824e+002
3.187e+002
2.550e+002
1.912e+002
1.275e+002
6.374e+001
0.000e+000
[m s^-1]
Type 4
1 MPa
Diamond shocks
0
0.01 (m)
0.005
Y
X

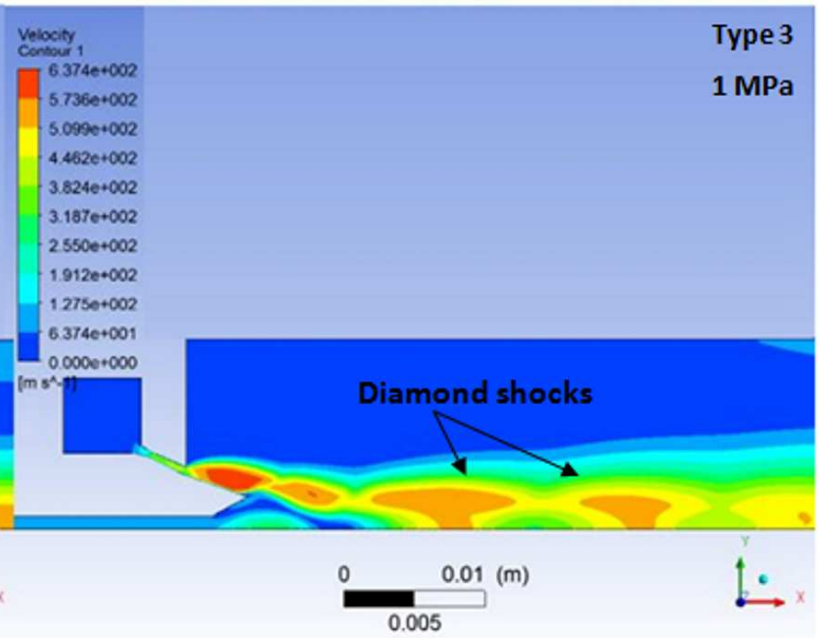
Velocity
Contour 1
6.374e+002
5.736e+002
5.099e+002
4.462e+002
3.824e+002
3.187e+002
2.550e+002
1.912e+002
1.275e+002
6.374e+001
0.000e+000
[m s^-1]
Type 3
1 MPa
Diamond shocks
0
0.01 (m)
0.005
Y
X

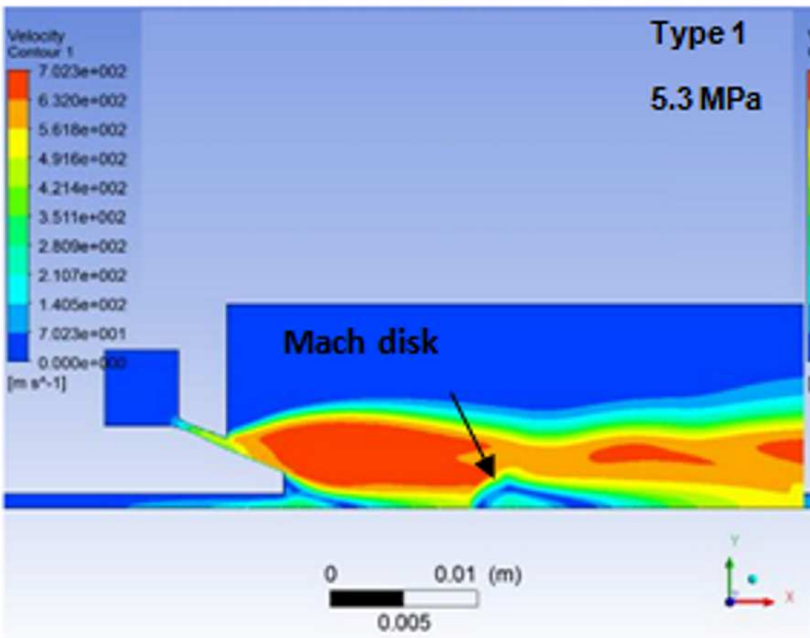
Type 1
5.3 MPa
Velocity
Contour 1
7.023e+002
6.320e+002
5.618e+002
4.916e+002
4.214e+002
3.511e+002
2.809e+002
2.107e+002
1.405e+002
7.023e+001
0.000e+000
[m s^-1]
Mach disk
0
0.01 (m)
0.005

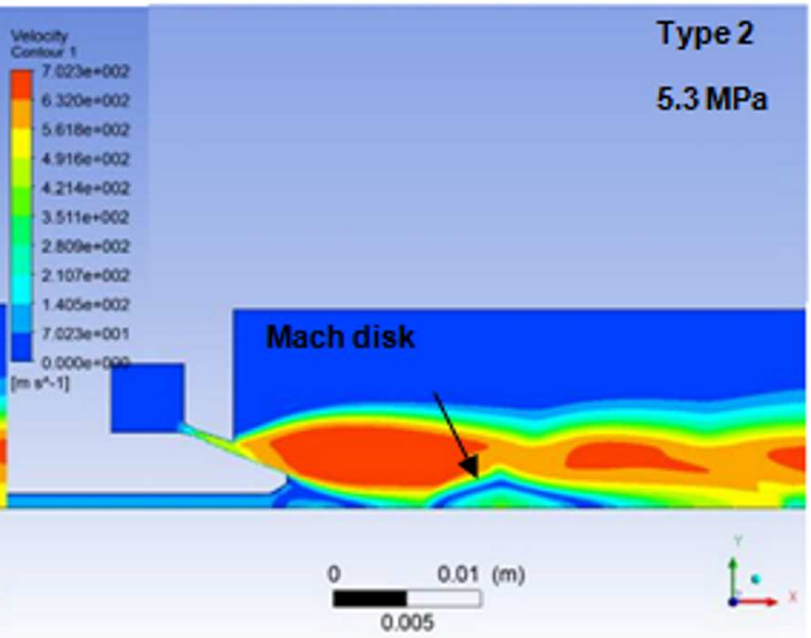
Type 2
5.3 MPa
Velocity
Contour 1
7.023e+002
6.320e+002
5.618e+002
4.916e+002
4.214e+002
3.511e+002
2.809e+002
2.107e+002
1.405e+002
7.023e+001
0.000e+000
[m s^-1]
Mach disk
0
0.01 (m)
0.005

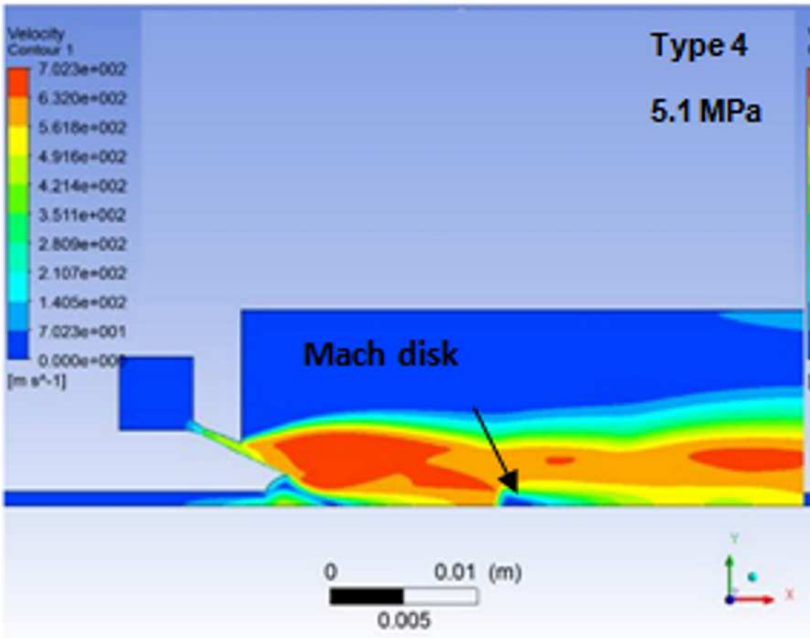
Type 4
5.1 MPa
Velocity
Contour 1
7.023e+002
6.320e+002
5.618e+002
4.916e+002
4.214e+002
3.511e+002
2.809e+002
2.107e+002
1.405e+002
7.023e+001
0.000e+000
[m s^-1]
Mach disk
0
0.01 (m)
0.005

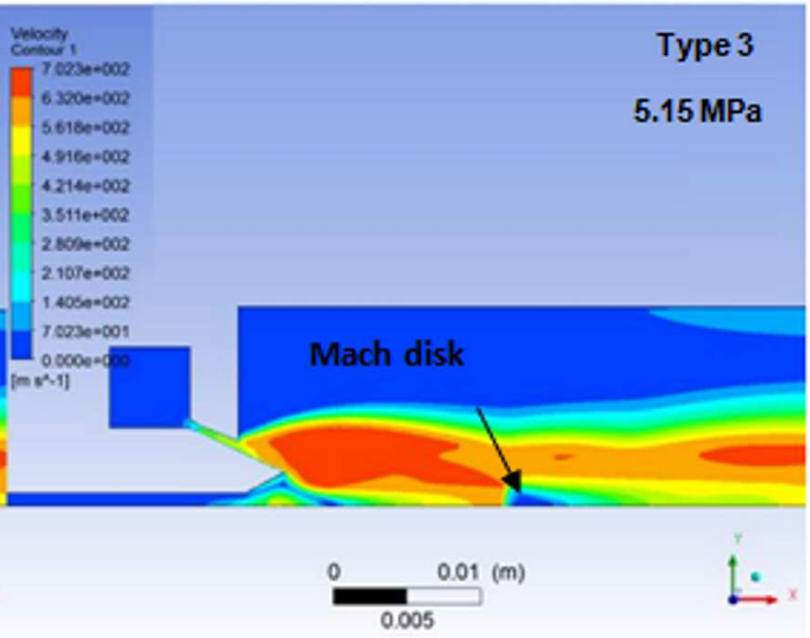
Type 3
5.15 MPa
Velocity
Contour 1
7.023e+002
6.320e+002
5.618e+002
4.916e+002
4.214e+002
3.511e+002
2.809e+002
2.107e+002
1.405e+002
7.023e+001
0.000e+000
[m s^-1]
Mach disk
0
0.01 (m)
0.005

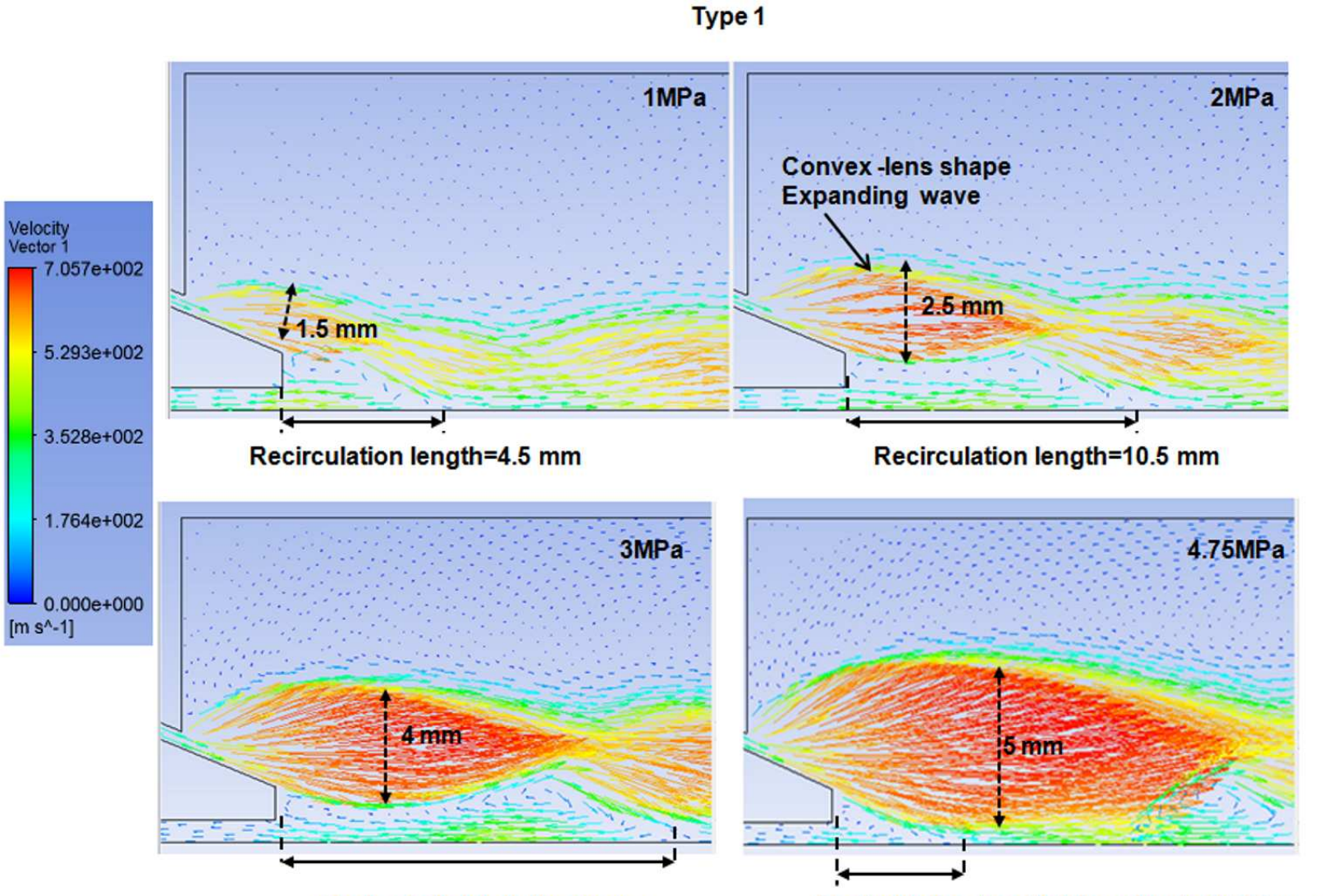
Type 1
1MPa
1.5 mm
Recirculation length=4.5 mm
2MPa
Convex -lens shape
Expanding wave
2.5 mm
Recirculation length=10.5 mm
Velocity
Vector 1
7.057e+002
5.293e+002
3.528e+002
1.764e+002
0.000e+000
[m s^-1]
3MPa
4 mm
Recirculation length=12 mm
4.75MPa
5 mm
Recirculation length (closed-wake)=3.5 mm

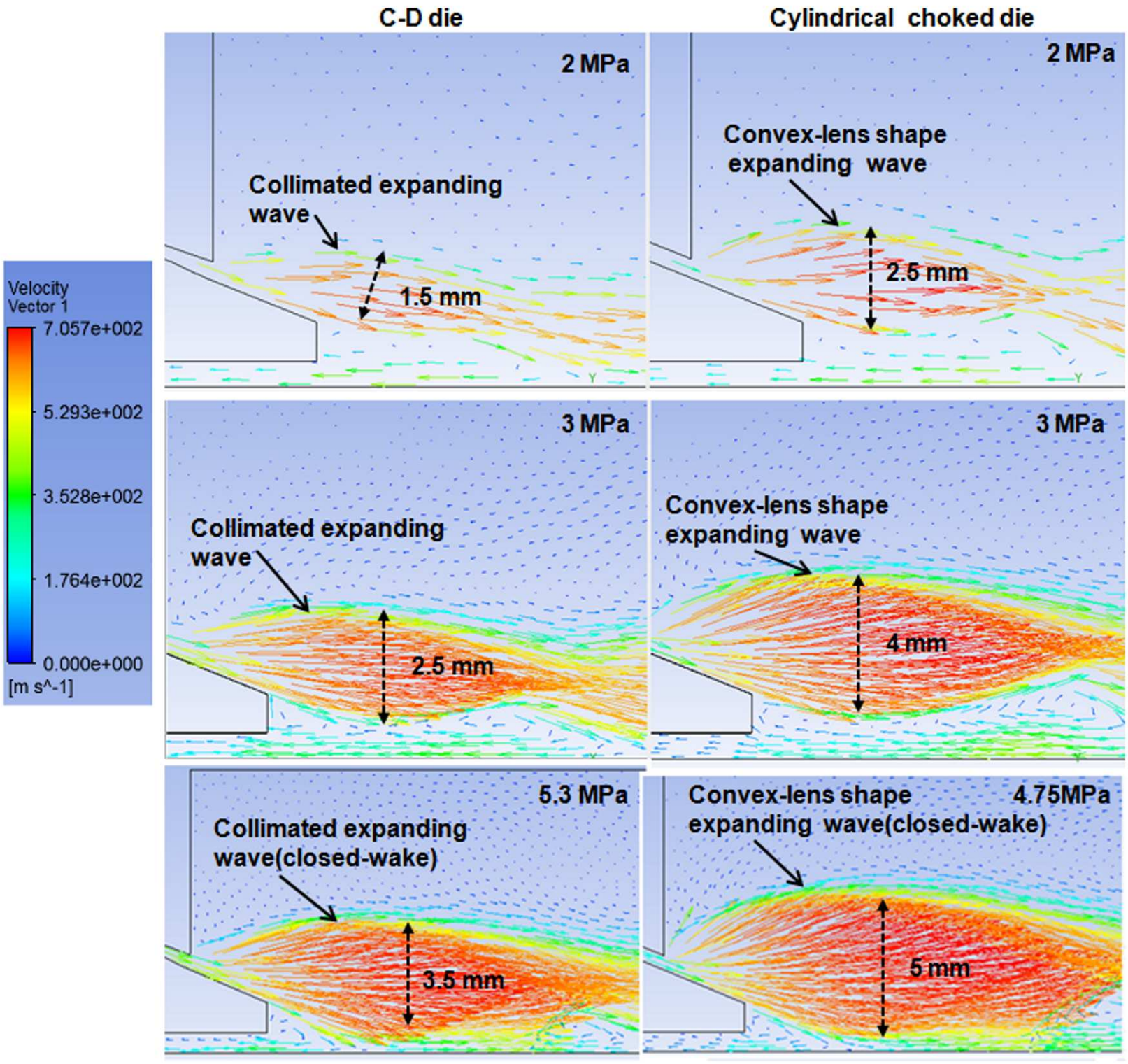
C-D die
Cylindrical choked die
2 MPa
Collimated expanding wave
1.5 mm
2 MPa
Convex-lens shape expanding wave
2.5 mm
Velocity Vector 1
7.057e+002
5.293e+002
3.528e+002
1.764e+002
0.000e+000
[m s^-1]
3 MPa
Collimated expanding wave
2.5 mm
3 MPa
Convex-lens shape expanding wave
4 mm
5.3 MPa
Collimated expanding wave(closed-wake)
3.5 mm
Convex-lens shape expanding wave(closed-wake)
4.75MPa
5 mm

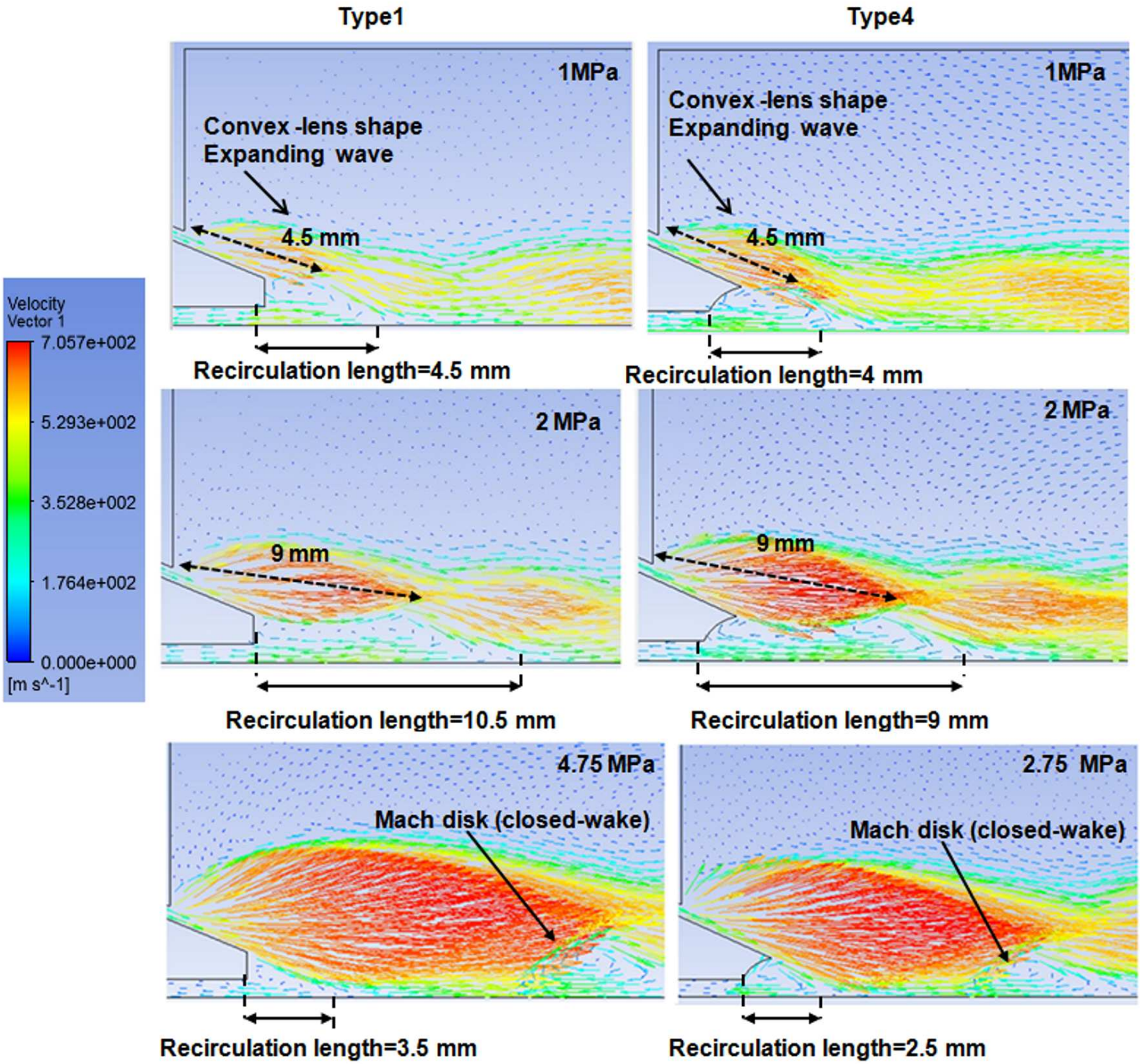
Type1
Type4
1MPa
Convex -lens shape
Expanding wave
4.5 mm
Recirculation length=4.5 mm
1MPa
Convex -lens shape
Expanding wave
4.5 mm
Recirculation length=4 mm
Velocity
Vector 1
7.057e+002
5.293e+002
3.528e+002
1.764e+002
0.000e+000
[m s^-1]
2 MPa
9 mm
Recirculation length=10.5 mm
2 MPa
9 mm
Recirculation length=9 mm
4.75 MPa
Mach disk (closed-wake)
Recirculation length=3.5 mm
2.75 MPa
Mach disk (closed-wake)
Recirculation length=2.5 mm

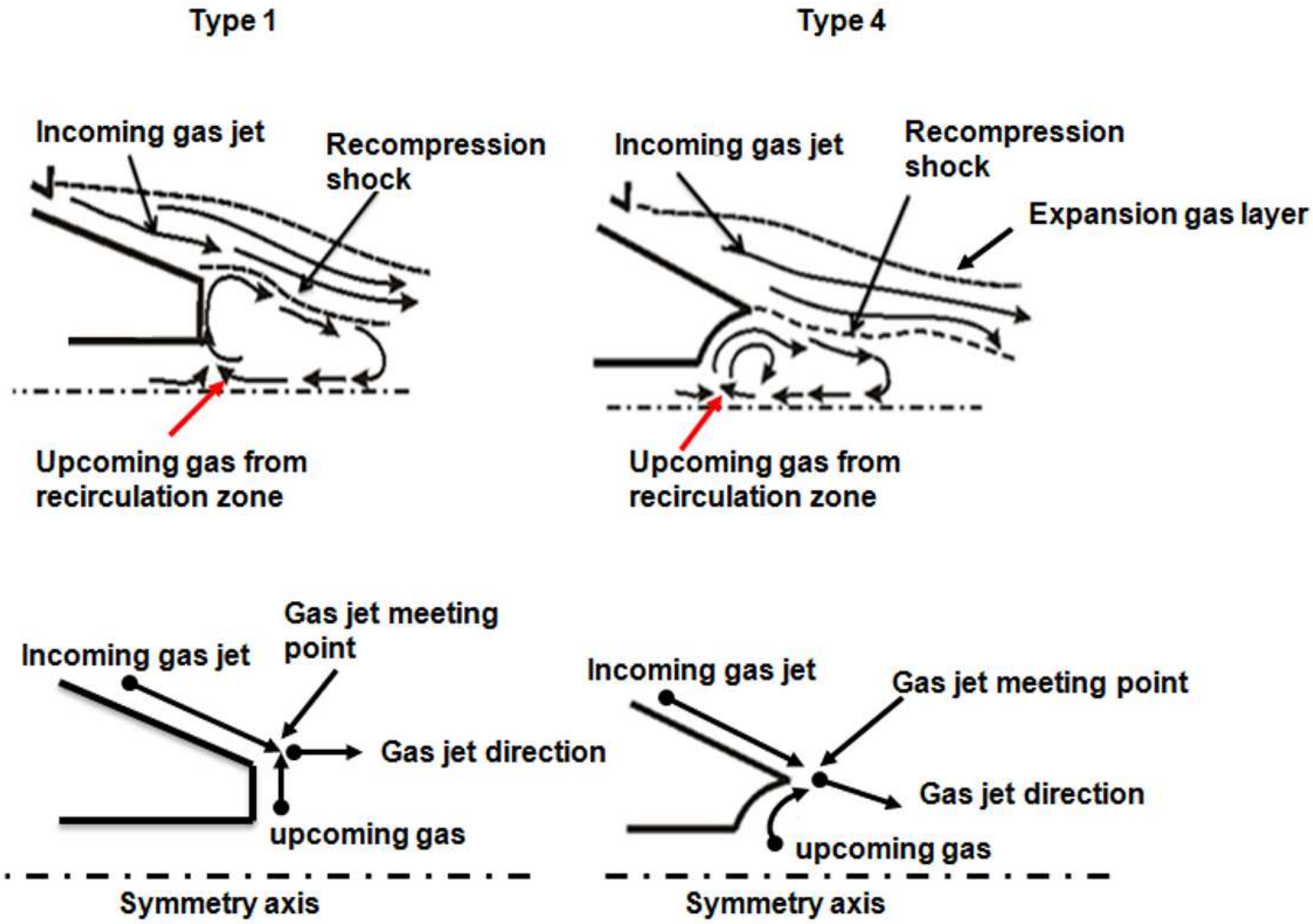
Type 1
Type 4
Incoming gas jet
Recompression shock
Upcoming gas from recirculation zone
Incoming gas jet
Recompression shock
Expansion gas layer
Upcoming gas from recirculation zone
Incoming gas jet
Gas jet meeting point
Gas jet direction
upcoming gas
Symmetry axis
Incoming gas jet
Gas jet meeting point
Gas jet direction
upcoming gas
Symmetry axis

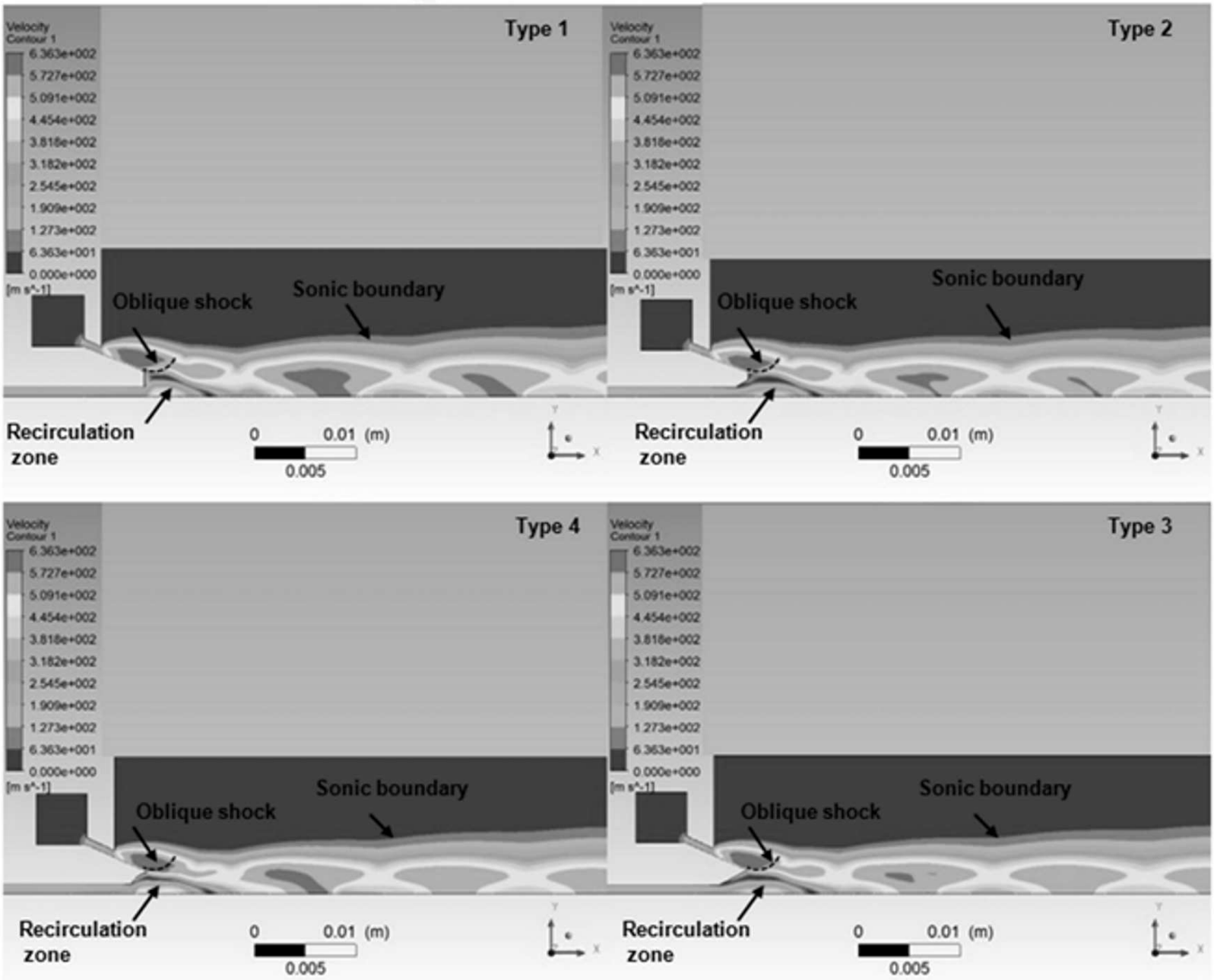
Type 1
Velocity
Contour 1
6.363e+002
5.727e+002
5.091e+002
4.454e+002
3.818e+002
3.182e+002
2.545e+002
1.909e+002
1.273e+002
6.363e+001
0.000e+000
[m s^-1]
Oblique shock
Sonic boundary
Recirculation zone
0
0.01 (m)
0.005
Type 2
Velocity
Contour 1
6.363e+002
5.727e+002
5.091e+002
4.454e+002
3.818e+002
3.182e+002
2.545e+002
1.909e+002
1.273e+002
6.363e+001
0.000e+000
[m s^-1]
Sonic boundary
Oblique shock
Recirculation zone
0
0.01 (m)
0.005
Type 4
Velocity
Contour 1
6.363e+002
5.727e+002
5.091e+002
4.454e+002
3.818e+002
3.182e+002
2.545e+002
1.909e+002
1.273e+002
6.363e+001
0.000e+000
[m s^-1]
Sonic boundary
Oblique shock
Recirculation zone
0
0.01 (m)
0.005
Type 3
Velocity
Contour 1
6.363e+002
5.727e+002
5.091e+002
4.454e+002
3.818e+002
3.182e+002
2.545e+002
1.909e+002
1.273e+002
6.363e+001
0.000e+000
[m s^-1]
Sonic boundary
Oblique shock
Recirculation zone
0
0.01 (m)
0.005

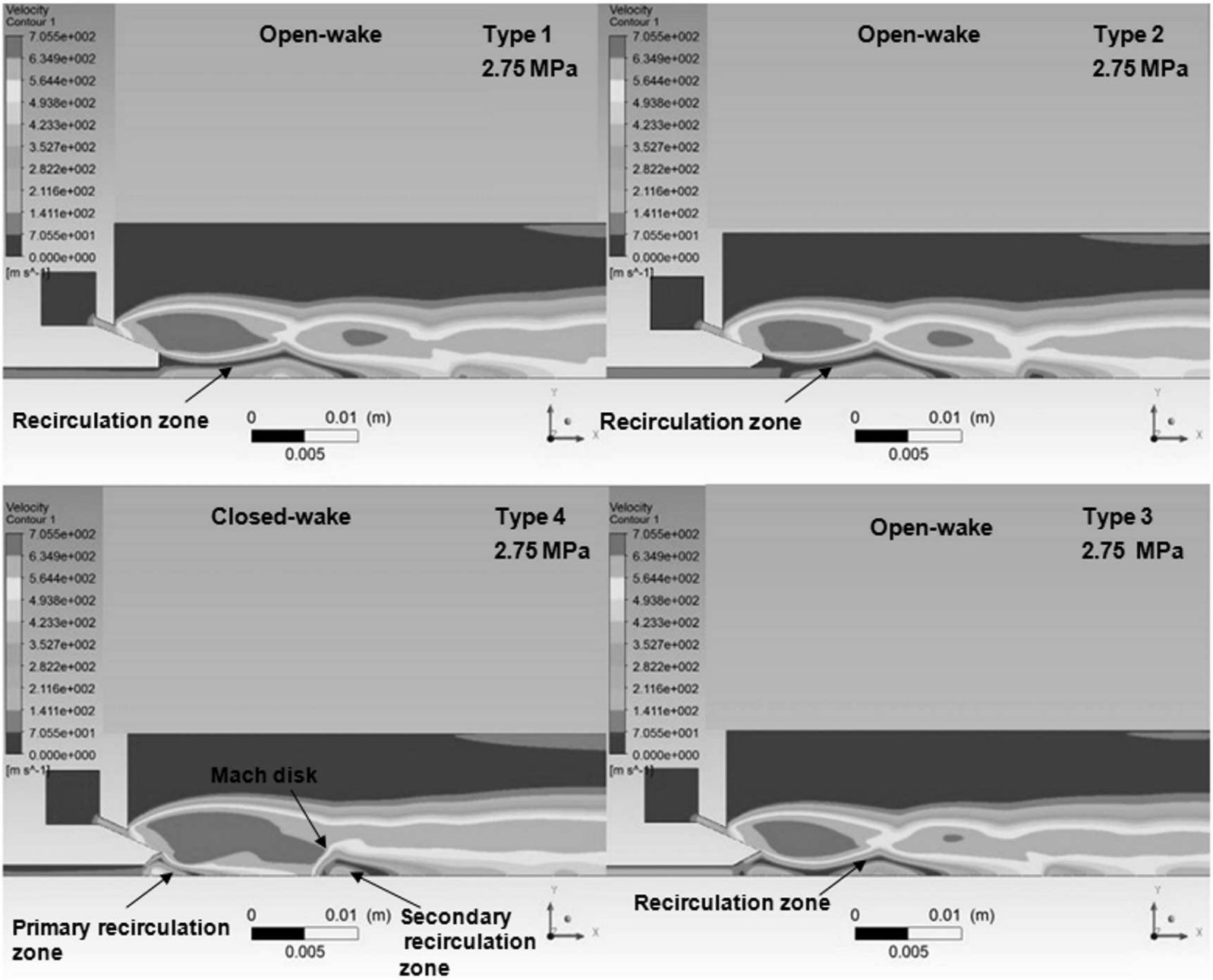
Velocity
Contour 1
7.055e+002
6.349e+002
5.644e+002
4.938e+002
4.233e+002
3.527e+002
2.822e+002
2.116e+002
1.411e+002
7.055e+001
0.000e+000
[m s^-1]
Open-wake
Type 1
2.75 MPa
Recirculation zone
0
0.01 (m)
0.005
Open-wake
Type 2
2.75 MPa
Recirculation zone
0
0.01 (m)
0.005
Closed-wake
Type 4
2.75 MPa
Mach disk
Primary recirculation zone
0
0.01 (m)
0.005
Secondary recirculation zone
Open-wake
Type 3
2.75 MPa
Recirculation zone
0
0.01 (m)
0.005

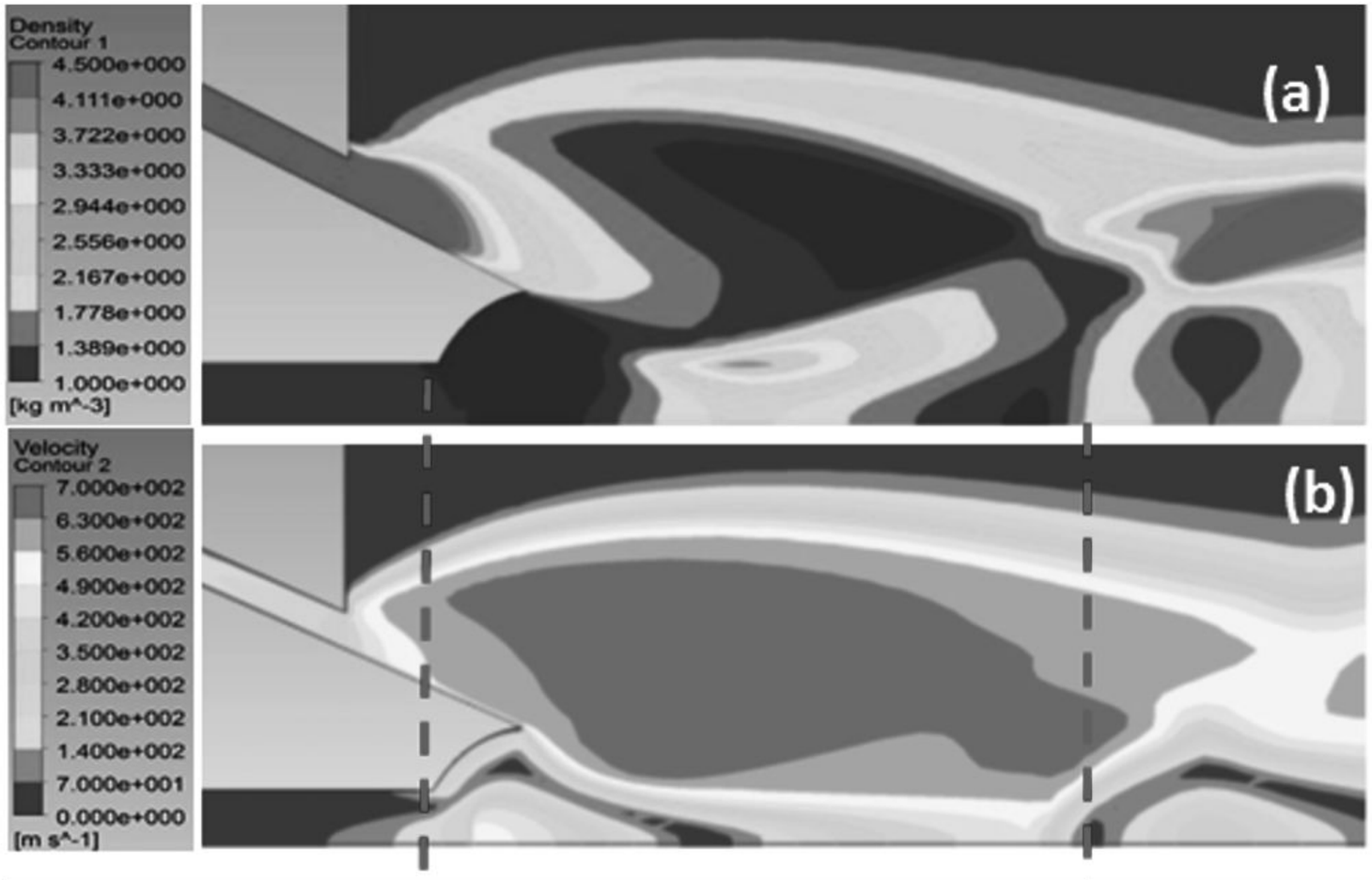
Density
Contour 1
4.500e+000
4.111e+000
3.722e+000
3.333e+000
2.944e+000
2.556e+000
2.167e+000
1.778e+000
1.389e+000
1.000e+000
[kg m^-3]
(a)
Velocity
Contour 2
7.000e+002
6.300e+002
5.600e+002
4.900e+002
4.200e+002
3.500e+002
2.800e+002
2.100e+002
1.400e+002
7.000e+001
0.000e+000
[m s^-1]
(b)

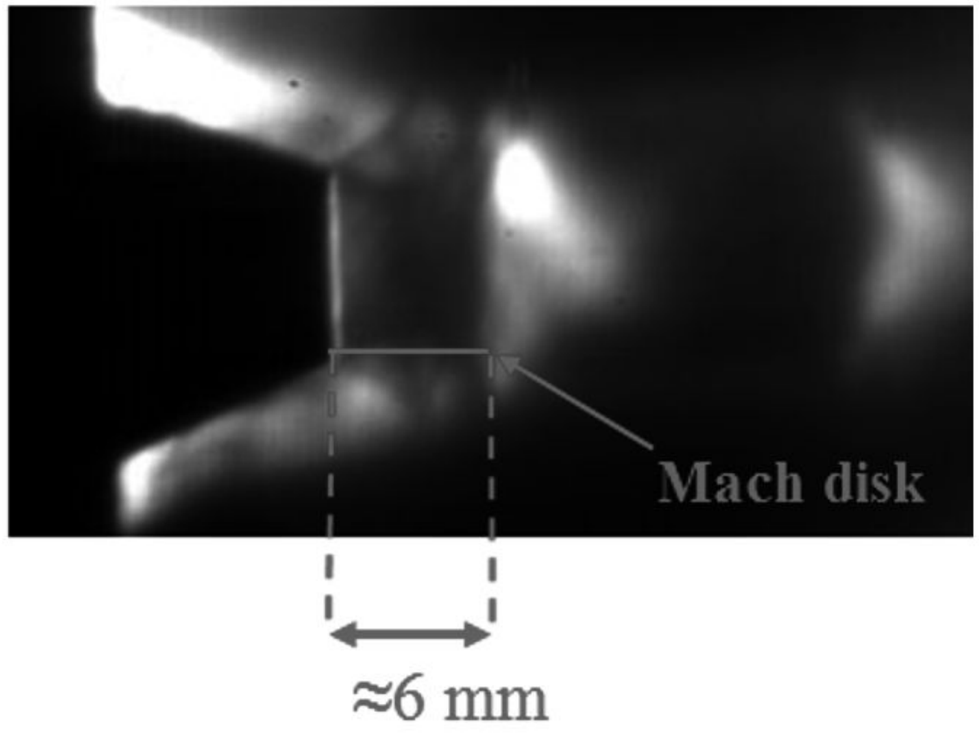
Mach disk
≈6 mm

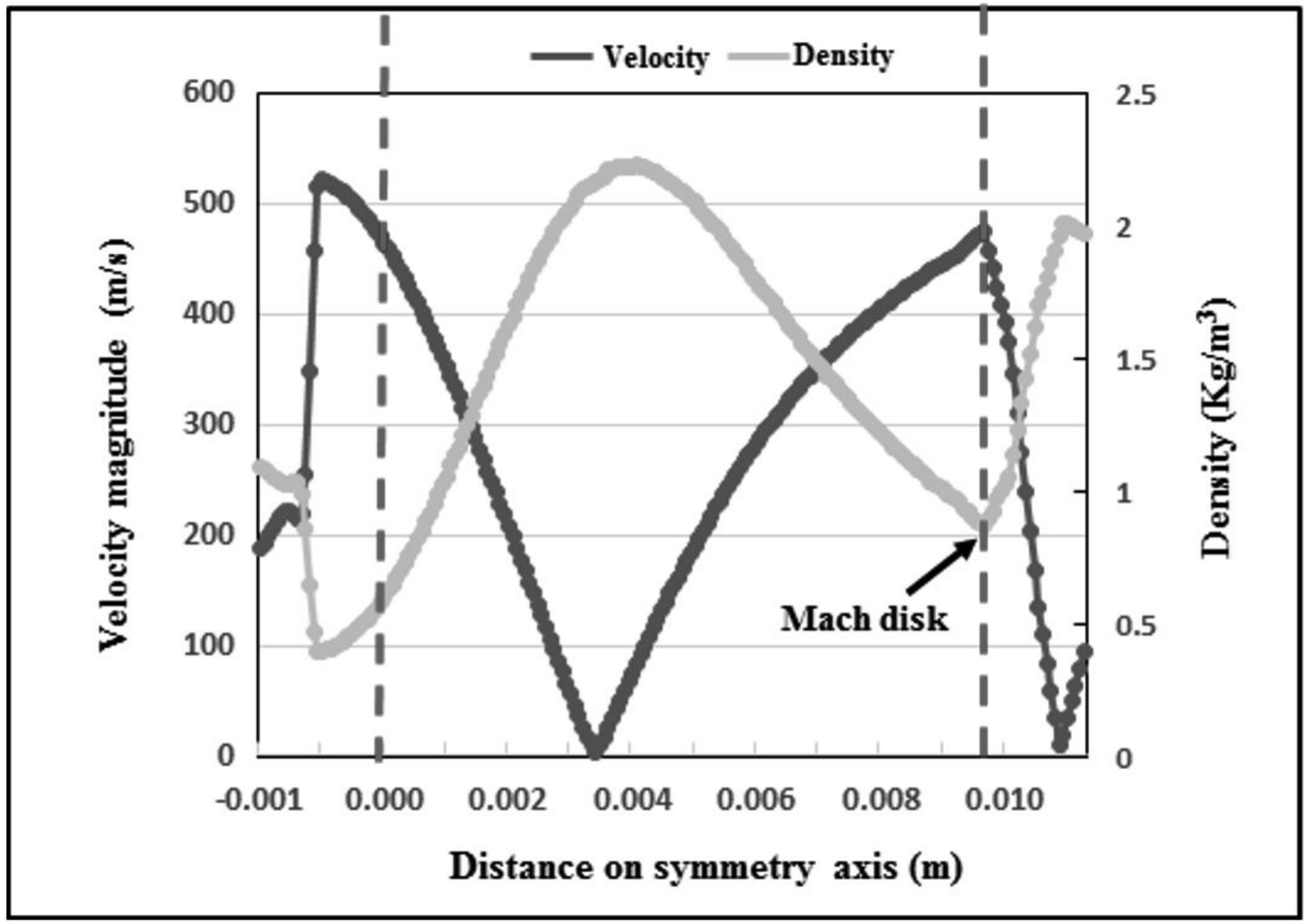
Velocity
Density
600
500
400
300
200
100
0
2.5
2
1.5
1
0.5
0
-0.001
0.000
0.002
0.004
0.006
0.008
0.010
Velocity magnitude (m/s)
Density (Kg/m3)
Mach disk
Distance on symmetry axis (m)

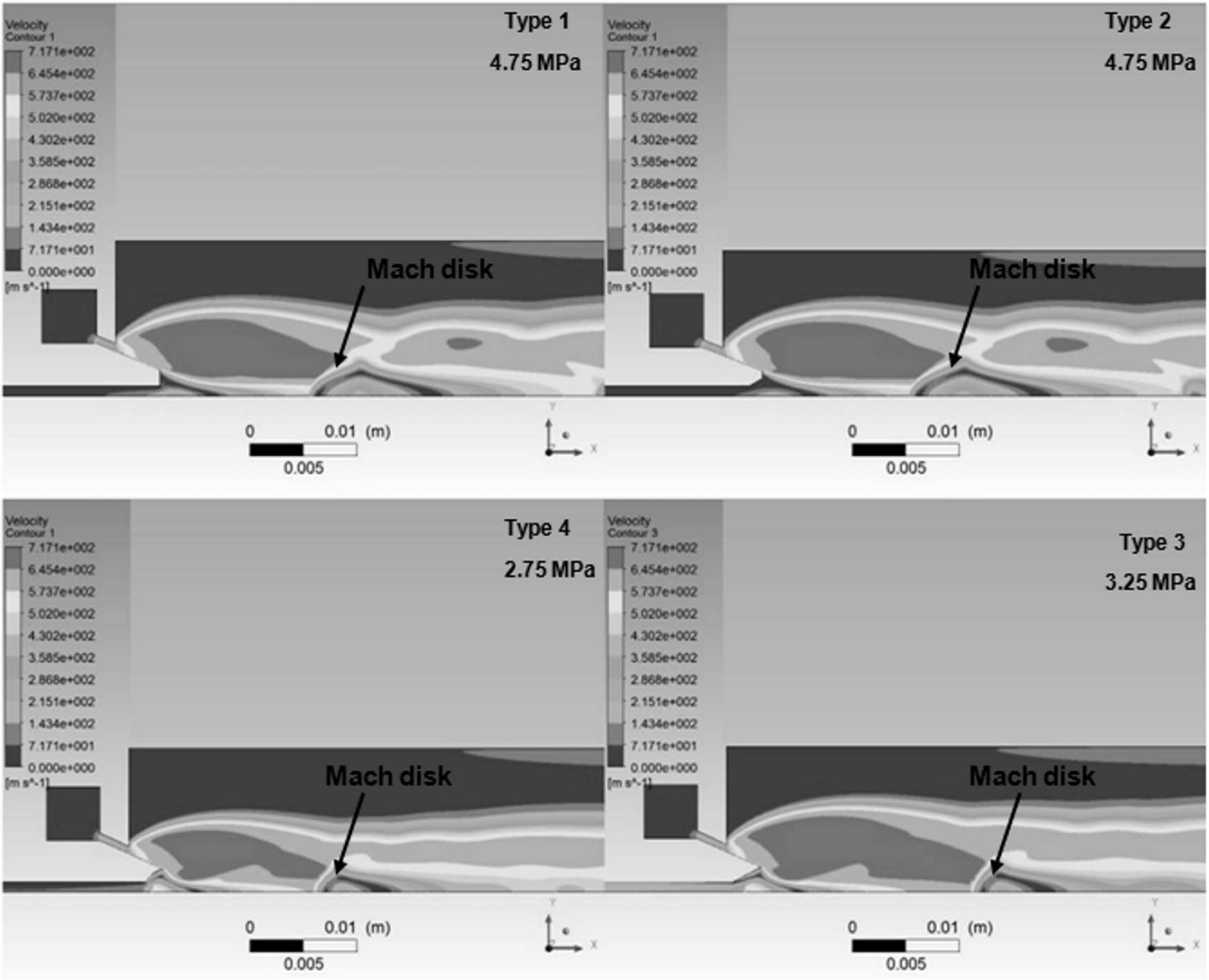
Type 1
4.75 MPa
Velocity
Contour 1
7.171e+002
6.454e+002
5.737e+002
5.020e+002
4.302e+002
3.585e+002
2.868e+002
2.151e+002
1.434e+002
7.171e+001
0.000e+000
[m s^-1]
Mach disk
0
0.01 (m)
0.005
Type 2
4.75 MPa
Velocity
Contour 1
Mach disk
Type 4
2.75 MPa
Velocity
Contour 1
Mach disk
Type 3
3.25 MPa
Velocity
Contour 3
Mach disk

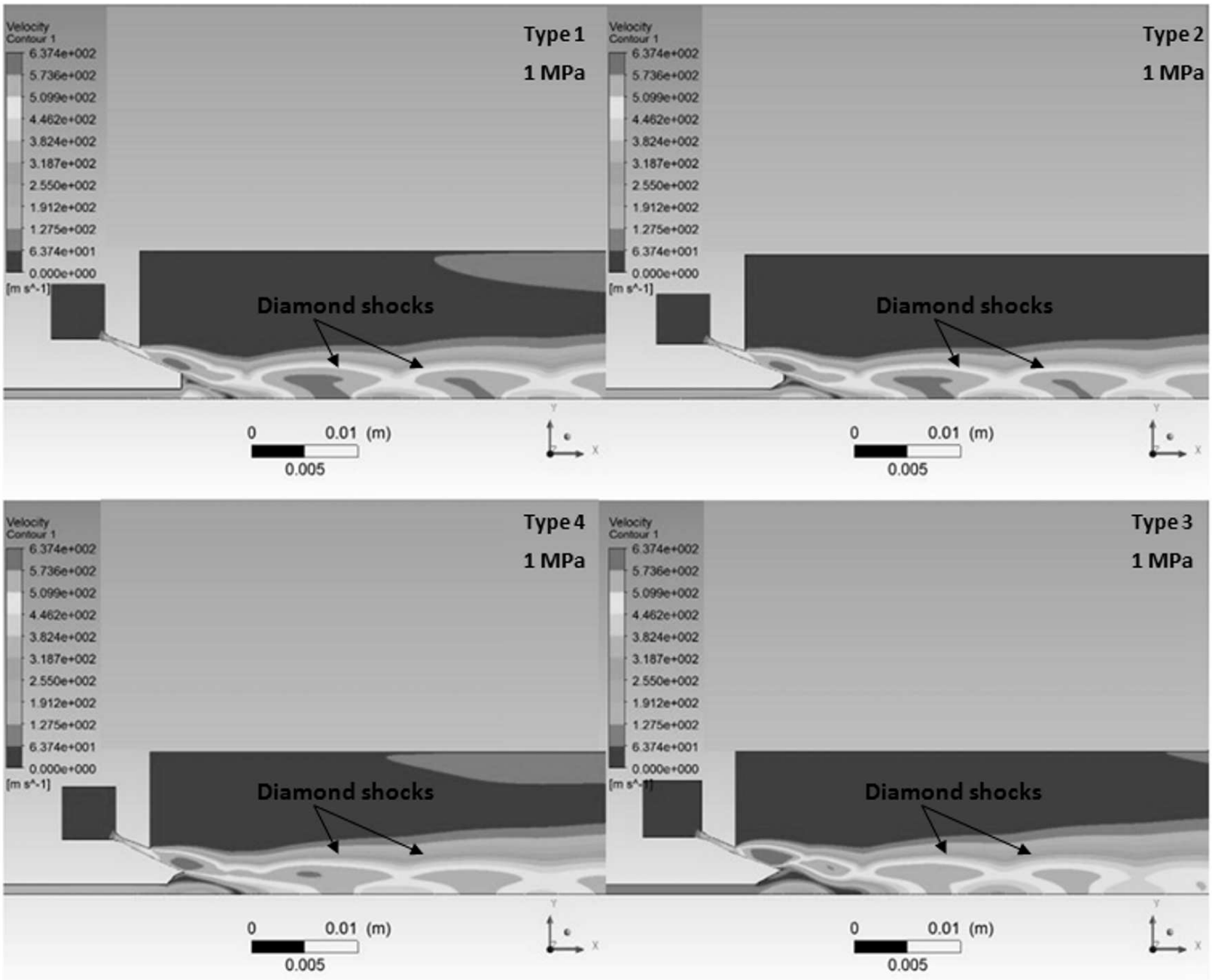
Velocity
Contour 1
6.374e+002
5.736e+002
5.099e+002
4.462e+002
3.824e+002
3.187e+002
2.550e+002
1.912e+002
1.275e+002
6.374e+001
0.000e+000
[m s^-1]
Type 1
1 MPa
Diamond shocks
0
0.01 (m)
0.005
Y
X
Type 2
1 MPa
Diamond shocks
Type 4
1 MPa
Diamond shocks
Type 3
1 MPa
Diamond shocks

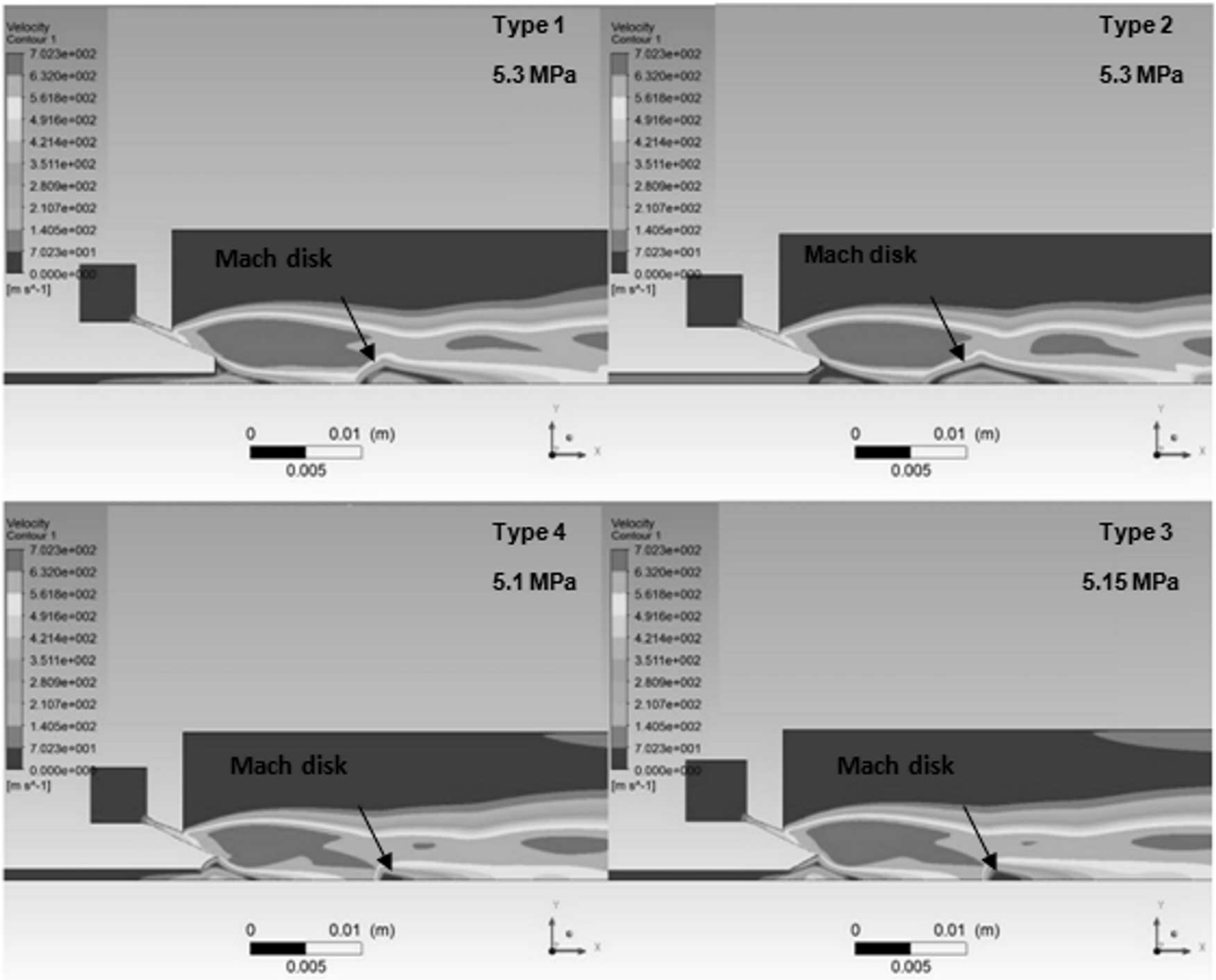
Type 1
5.3 MPa
Mach disk
Type 2
5.3 MPa
Mach disk
Type 4
5.1 MPa
Mach disk
Type 3
5.15 MPa
Mach disk
Velocity
Contour 1
7.023e+002
6.320e+002
5.618e+002
4.916e+002
4.214e+002
3.511e+002
2.809e+002
2.107e+002
1.405e+002
7.023e+001
[m s^-1]
0
0.01 (m)
0.005

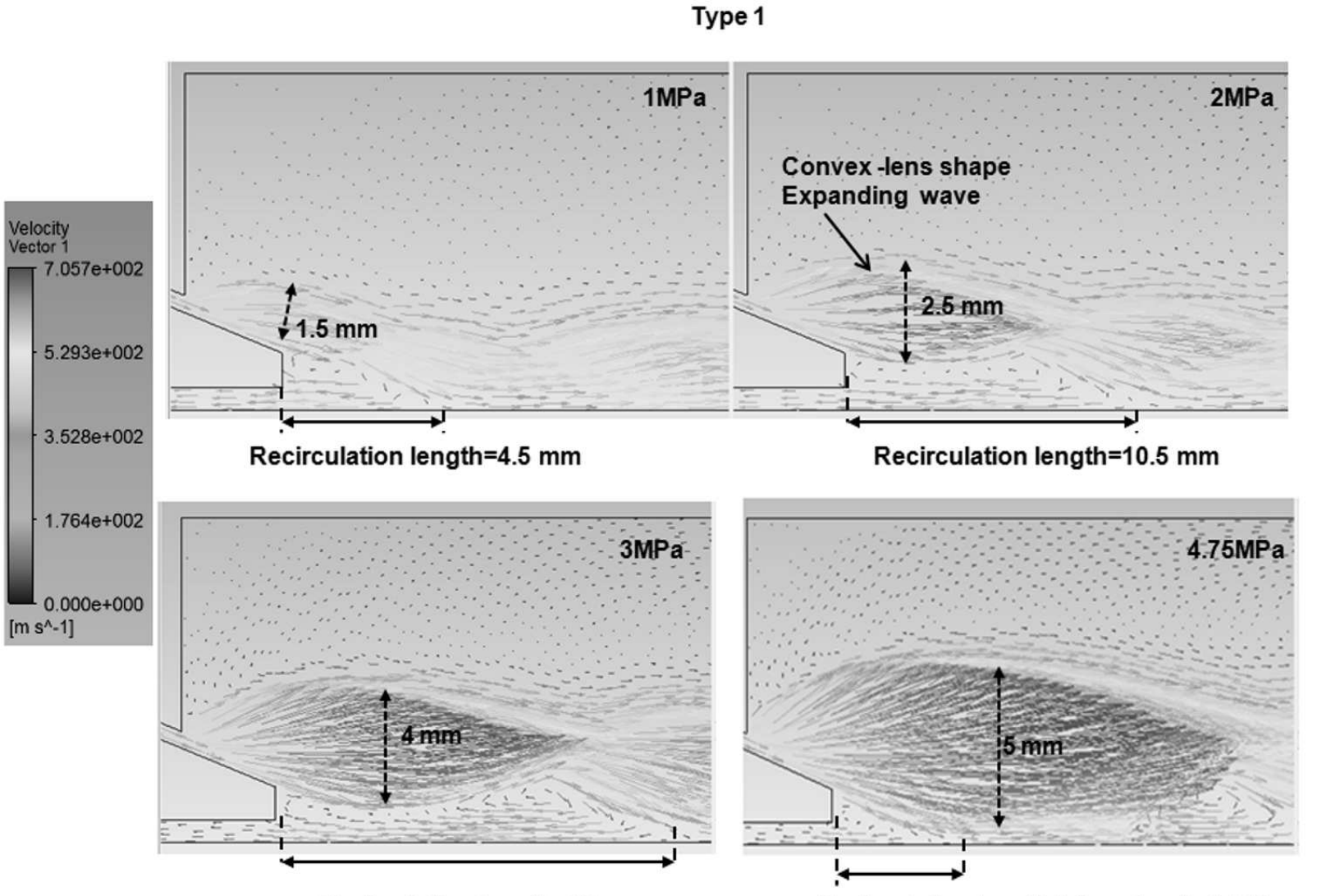
Type 1
Velocity
Vector 1
7.057e+002
5.293e+002
3.528e+002
1.764e+002
0.000e+000
[m s^-1]
1MPa
1.5 mm
Recirculation length=4.5 mm
2MPa
Convex -lens shape
Expanding wave
2.5 mm
Recirculation length=10.5 mm
3MPa
4 mm
Recirculation length=12 mm
4.75MPa
5 mm
Recirculation length (closed-wake)=3.5 mm

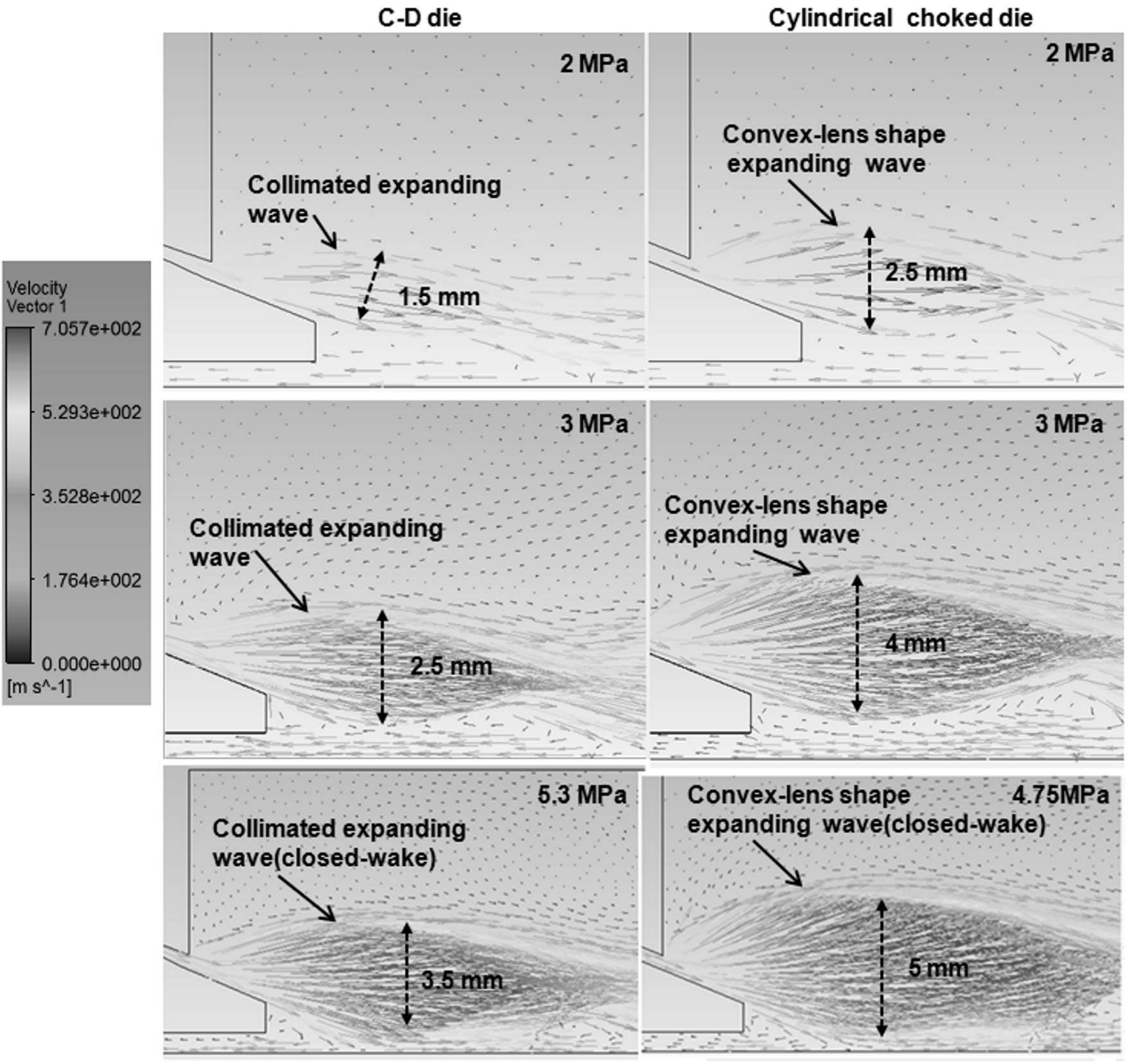
C-D die
Cylindrical choked die
2 MPa
Collimated expanding wave
1.5 mm
2 MPa
Convex-lens shape expanding wave
2.5 mm
Velocity Vector 1
7.057e+002
5.293e+002
3.528e+002
1.764e+002
0.000e+000
[m s^-1]
3 MPa
Collimated expanding wave
2.5 mm
3 MPa
Convex-lens shape expanding wave
4 mm
5.3 MPa
Collimated expanding wave(closed-wake)
3.5 mm
Convex-lens shape expanding wave(closed-wake)
4.75MPa
5 mm

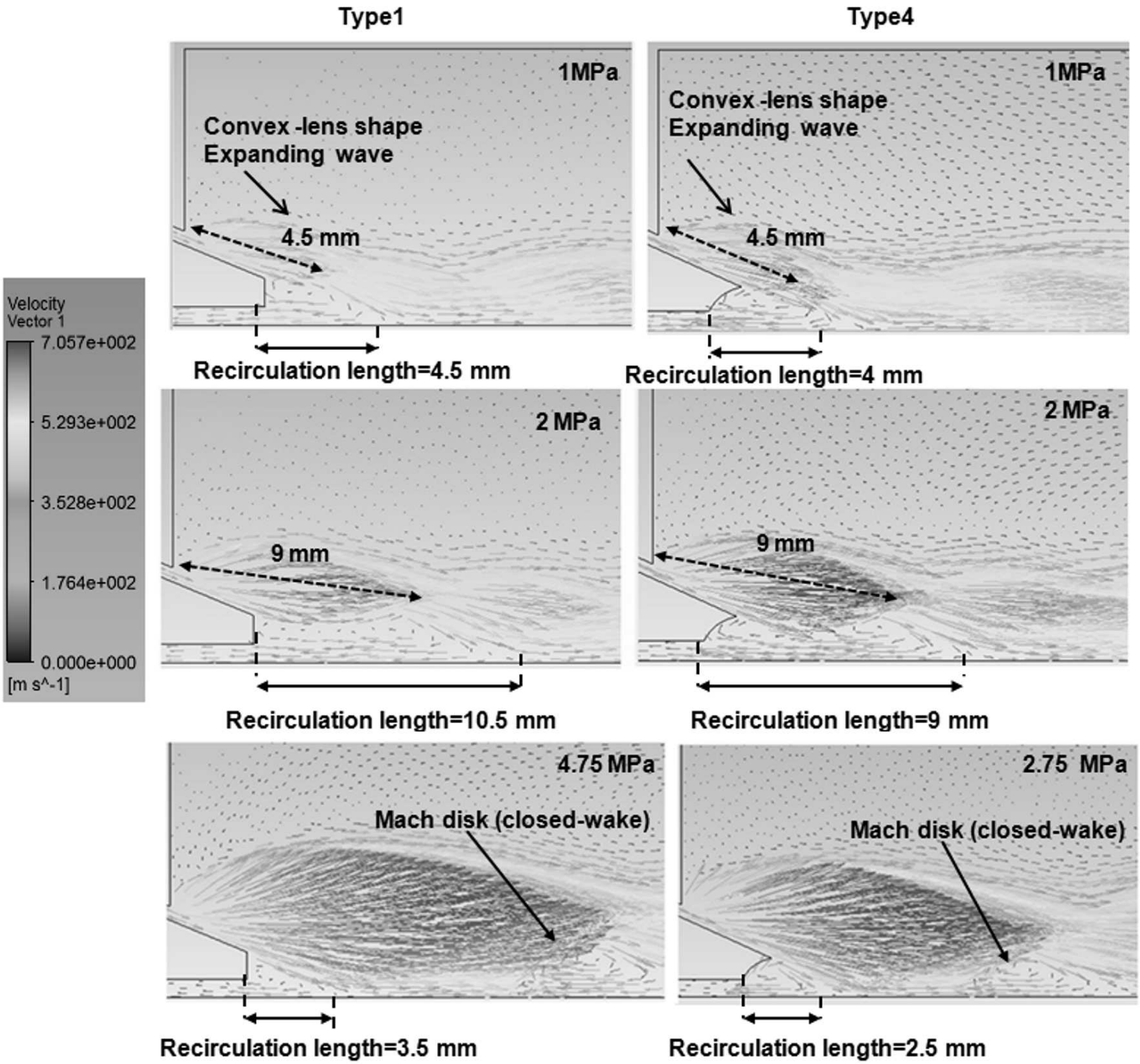
Type1
Type4
1MPa
Convex -lens shape
Expanding wave
4.5 mm
Recirculation length=4.5 mm
1MPa
Convex -lens shape
Expanding wave
4.5 mm
Recirculation length=4 mm
Velocity
Vector 1
7.057e+002
5.293e+002
3.528e+002
1.764e+002
0.000e+000
[m s^-1]
2 MPa
9 mm
Recirculation length=10.5 mm
2 MPa
9 mm
Recirculation length=9 mm
4.75 MPa
Mach disk (closed-wake)
Recirculation length=3.5 mm
2.75 MPa
Mach disk (closed-wake)
Recirculation length=2.5 mm

Melt nozzle type / Gas die type	Type 1	Type 2	Type 3	Type 4
Cylindrical die at experimental	4.5 (MPa)	4.5 (MPa)	3.5 (MPa)	3 (MPa)
Cylindrical die at CFD	4.75 (MPa)	4.75 (MPa)	3.25 (MPa)	2.75 (MPa)
C-D die at CFD	5.3 (MPa)	5.3 (MPa)	5.15 (MPa)	5.1 (MPa)